Electrokinetic remediation of estuarine sediments using a large reactor: spatial variation of physicochemical, mineral, and chemical properties

Hussein J Kanbar, Ahmad Zein-Eddin, Mohamed-Tahar Ammami, Ahmed Benamar

DOI: 10.1007/s11356-023-30271-8
Published in Environmental Science and Pollution Research

Electrokinetic remediation of estuarine sediments using a large reactor: Spatial variation of physicochemical, mineral, and chemical properties

Hussein J. Kanbar*, Ahmad Zein-Eddin, Mohamed-Tahar Ammami*, Ahmed Benamar

Laboratoire Ondes et Milieux complexes (LOMC), UMR 6294 CNRS, University of Le Havre Normandy (ULHN), 76600 Le Havre, France. A.B: ahmed.benamar@univ-lehavre.fr; A.Z: ahmad.zein-eddin@univ-lehavre.fr

* Correspondence: Hussein J. Kanbar, Hsen.kanbar@gmail.com, ORCID 0000-0002-9505-9974; Mohamed-Tahar Ammami, mohamed-tahar.ammami@univ-lehavre.fr

Abstract

The treatment and beneficial use of polluted or contaminated environmental matrices have become major issues, especially as the world strives toward a zero-waste policy. In this regard, dredged sediments need to be treated before they can be used in an environmentally safe and sustainable manner. Therefore, this work aims to treat estuarine sediments and, more importantly, use physicochemical, mineral, organic, and chemical information to understand the reactions that occur upon treatment. Dredged estuarine sediments were collected from Tancarville (Seine River estuary, France) and subjected to electrokinetic (EK) remediation using a 128 L laboratory-scale reactor. The sediments were treated 8 hrs per day for 21 days. The electric (voltage and current) and physicochemical (pH and electric conductivity) parameters were monitored during treatment. Sediments were collected from various sections in the reactor at the end of the experiment (lengthwise, widthwise, and depthwise). The spatial variation was investigated in terms of organic, mineral, and metal contents. Statistical analyses proved that the variation occurred only in the lengthwise direction. Furthermore, three main phases described the treatment, which were mainly linked to carbonate dissolution and pH variation. The results also showed that the trace elements Ni and Zn were reduced by 21% and 19%, respectively, without a direct link to pH, while Ca and Mg were only redistributed. The buffering capacity of the anodic sediment was reduced due to carbonate dissolution. The treated sediments showed reduced contents in trace metals without affecting major elements that can be useful in agriculture (i.e., Ca and Mg).

Keywords: dredged sediments, remediation, environmental sustainability, circular economy, carbonates, metal behavior

1. Introduction

The introduction of contaminants and pollutants to environmental matrices hinders the attainment of a sustainable environment. Such environmental concerns can be overcome by reusing matrices after adequate treatment. Sediments represent one of these matrices. In principle, sediments contain the same components as soils, since the former is generally a weathering product of the latter. However, sediment particles are usually finer and therefore have a relatively higher surface area, which in turn allow them to sorb natural as well as anthropogenic substances, such as metals and organics (e.g., Owens et al. 2005; Marshak 2011). The unwanted substances in environmental matrices can be removed or reduced through electrokinetic remediation (EKR, or EK for electrokinetic). Indeed, this technique overcomes the fine texture and has been successfully proven to treat sediments and other environmental matrices (e.g., Acar and Alshawabkeh 1993; Wen et al. 2021a). Nonetheless, the success and efficiency of treatment depend on the running parameters (e.g., voltage), EK reactor size, electrode position and geometry, chelating agents, and the matrix itself on the one hand, and the physico-chemical and mineral reactions that occur in the matrix on the other (e.g., Li et al. 2014; Ammami et al. 2015; Han et al. 2021). Therefore, the achievement of efficient treatment relies on the consideration of all these interdependent parameters.

It has been proven that a 0.5 – 2 V/cm range is an efficient and economically-friendly way to treat matrices (e.g., Gomes et al. 2012; Huang et al. 2015). Furthermore, the spatial distribution and variation of physicochemical parameters (e.g., pH, oxidoreduction potential "ORP", and electric conductivity "EC") and metal contents are important criteria when relatively large EK reactors are used and/or if small EK reactors are scaled-up (e.g., Li et al. 2009; Benamar et al. 2020). When metal-rich media are treated, the choice of a chelating agent, i.e., an organic acid, depends on the metals that need to be removed since metal species have different affinities to organic acids (e.g., Song et al. 2016; Kanbar et al. 2020). Citric acid is naturally produced by plant roots (root exudates) to manage nutrient uptake (Chen et al. 2017). It is also environmentally safe, biodegradable, and present in anionic forms in most pH ranges, thus serving as an efficient chelating agent in EKR (e.g., Yeung and Gu 2011; Benamar et al. 2019; Wen et al. 2021a).

Although metal speciation and migration largely depend on the species, sedimentary (or soil) components affect metal behavior (sorption/release) through various chemical and mineral processes. Furthermore, metal behavior and toxicity are different between spiked and natural matrices due to the variation in speciation (e.g., McBride et al. 2009; Neaman et al. 2020); thus, metal removal efficiency in spiked matrices, by EKR or others, does not represent that of lithogenic or anthropogenic ones. Moreover, carbonate minerals play a significant role in metal behavior since they buffer the medium (e.g., sediment) which in turn can limit reaching a favorable pH for metal removal (i.e., acidic). Carbonate dissolution raises the ionic strength or EC of the porewater by releasing calcium ions, which in turn compete with surface-bound metals and cause their release (e.g., Du Laing et al. 2008; Butler 2009; Acosta et al. 2011; Kanbar and Kaouk 2019). The effect of carbonates and the role of buffering capacity on the performance of EKR has mainly been studied in modeled soils or homogeneous clay minerals (e.g., Ouhadi et al. 2010; López-Vizcaíno et al. 2017, 2019), but rarely in natural materials due to their complexity. On that note, the behavior of metals as a result of EKR and their link to the running parameters have been

DOI: 10.1007/s11356-023-30271-8
Published in Environmental Science and Pollution Research

a challenge to understand in heterogeneous materials. To our knowledge, the impact of carbonates on metal behavior during EKR has not been studied in natural sediments. Furthermore, oxides and oxyhydroxides affect metal behavior by scavenging freely available ions, especially during their precipitation (e.g., Lynch et al. 2014). The effect of ionic strength on metal release is prominent in saline media, such as estuarine and marine sediments (Du Laing et al. 2008, 2009). Moreover, the removal or reduction of salts from estuarine sediments is necessary if the treated material is used in agriculture (Wen et al. 2021a). The elements that are targeted in EKR depend on the intended application of the treated materials. In general, unwanted and potentially toxic trace elements (e.g., As, Cd, Ni, Pb, and Sr) are targeted (e.g., Karaca et al. 2016; Ammami et al. 2022). On the other hand, macro-nutrients (e.g., Ca, Mg, Na, and P) and minerals that buffer the medium (e.g., carbonates) are usually not targeted and are better maintained in case the treated sediment is used in agriculture (e.g., Kiani et al. 2021).

Sediments from harbors, rivers, channels, and other waterbodies are periodically dredged to maintain a suitable water level for the safe transfer of ships. For example, between 100 and 200 million m^3 are annually dredged in Europe (Apitz 2010; Bose and Dhar 2022). A big part of these sediments is transferred to fill-in basins or dumped into the sea if the materials are considered harmless (LIFE SEDI.PORT.SIL 2021). Nonetheless, dredged sediments are considered as waste materials once deposited on land and do not follow the same regulations as polluted soils (EU 2008a, b). Unfortunately, only a small part is used or recycled as part of reaching a circular economy or attaining environmental sustainability (Torrance et al. 2008). Dredged sediments can be used in agriculture as amendments, in habitats as environmental enhancements, and in construction as building materials (e.g., Apitz 2010; Ketelaars et al. 2013; Interreg ReCon Soil 2022). In this framework, the aim is to eventually reduce wastes and incorporate such materials in environmentally safe and friendly manners. Treating dredged sediments using EKs is one approach to accomplish this. The treatment of estuarine sediments through EK has been challenging due to the complexity and heterogeneity of sediments on the one hand, and the presence of salts that can affect remediation efficiency on the other (Altaee et al. 2008; Pedersen et al. 2021). This work is part of the Interreg project "ReCon Soil" which has the objective of treating "waste" environmental matrices, such as dredged sediments and quarry sludge. These materials are then formulated into reconstructed soils for agricultural use (Interreg ReCon Soil 2022). The project aims to minimize waste, establish a circular economy, and eventually attain environmental sustainability. Therefore, the aim of this work is to treat natural and complex dredged sediments and use electrical and physicochemical information to understand the processes that occur during EKR on the one hand, and link this information to mineral and chemical processes on the other. Additionally, a statistical approach was used to elucidate those processes, which can be used to treat other matrices even if they have different compositions.

2. Materials and methods

2.1. Sediment collection, EKR reactor, and running parameters

Estuarine sediments were directly collected during a dredging operation at Tancarville (upper estuary of the Seine River, France) using a clamshell dredger. The fresh sediments were directly transported to the laboratory, mixed for homogenization, and loaded into a 128 L EKR reactor. The reactor contains two sediment compartments (L and R) of 40 x 40 x 40 cm dimensions (*Fig 1*a). The two compartments act as experimental replicates (Supplementary materials, *SM 1*). The two sediment compartments have a common anode electrode chamber and two cathode electrode chambers (*Fig 1*a). The dimensions of each chamber are 5 x 40 x 40 cm (i.e., 8 L capacity). Between the chambers and the sediment compartments are 31 x 26 perforated plates (1 cm diameter). Geotextile membranes were put along the inner walls of the sediment compartments to prevent particle movement to the electrolyte chambers. The inlet tubes for the electrolyte chambers are positioned 1 cm above the bottom and the outlet tubes are positioned 2 cm below the top. The sediments had a silty texture and were rich in organic matter (OM) and carbonates; other characteristics are included in *Table 1*. Graphite electrodes (10 x 20 x 1 cm) were used in the electrolyte chambers and connected to a DC power supply and an ammeter (to monitor the electric parameters). The voltage gradient was first set to 1 V/cm (i.e., 40 V), but the decline in resistance in less than one day then caused the current to increase to the generator's maximum limit (5.5 A, i.e., current density of 1.7 mA/cm^2 per compartment). After that point, the decline in resistance was balanced by a decline in voltage. In any case, a direct current (DC) was periodically applied for 21 days, 8 hrs per day. Citric acid (0.1 M, 2.36 pH, and 3.2 mS/cm EC) was used as an electrolyte in the cathode chambers (*Fig 1*a). The liberation of OH^- in the cathode chamber and consequently high pH promotes the formation of $citrate^{-3}$, which is then mobilized toward the anode electrode due to difference in charge. The electrolyte flow rate that supplied the electrode chambers was initially set at 10 mL/h. However, the temperature reached elevated levels during treatment, especially during the first days, which caused part of the electrolytes to evaporate. So, the anode and cathode chambers were filled with ultrapure water and citric acid (0.1 M), respectively, daily before starting the experiment. As a result, the electroosmotic flow could not be determined. It is worth noting that the electrolyte levels did not fall below the sediment level during treatment, thus keeping the sediments well-saturated with the electrolytes.

2.2. Direct measurements in the electrolyte chambers

The physicochemical properties (namely EC, pH, ORP, and temperature) in the anode and cathode chambers were collected twice per day for 21 days, i.e., at the start and end of the daily 8 hr electric current application (named daily starting and daily final, respectively). The EC and pH were measured using a HI5521 multimeter (from HANNA instruments) equipped with HI76312 (EC) and HI1131 (pH) electrodes, respectively; the temperature was monitored using a temperature probe. Oxidoreduction potential (ORP) was recorded using a PHM220 multimeter equipped with a combined platinum-Ag/AgCl redox electrode (HI4430B, from HANNA instruments).

2.3. Direct measurements in the sediment compartments

After 21 days of treatment, the pH and ORP were

DOI: 10.1007/s11356-023-30271-8
Published in Environmental Science and Pollution Research

directly measured in the sediment sections along the anode-cathode direction (lengthwise; represented by dots in *Fig 1*b), at variable positions away from the walls adjacent to the electrodes (widthwise, y1: 0 – 13.3 cm, y2: 13.3 – 26.6 cm, and y3: 26.6 – 40 cm), and as a function of depth (depthwise, z1: 0 – 13.3 cm, z2: 13.3 – 26.6 cm, and z3: 26.6 – 40 cm). The same sampling strategy was applied to the L and R compartments (*Fig 1*). These measurements were taken to investigate the reproducibility of the two sediment compartments and to study the spatial variation caused by EKR. The pH was directly measured using a PHM220 multimeter equipped with an L6880 pH electrode (Schott instruments) and the ORP was measured using the same equipment as stated above; more information on ORP measurement method is included elsewhere (Eijkelkamp 2009).

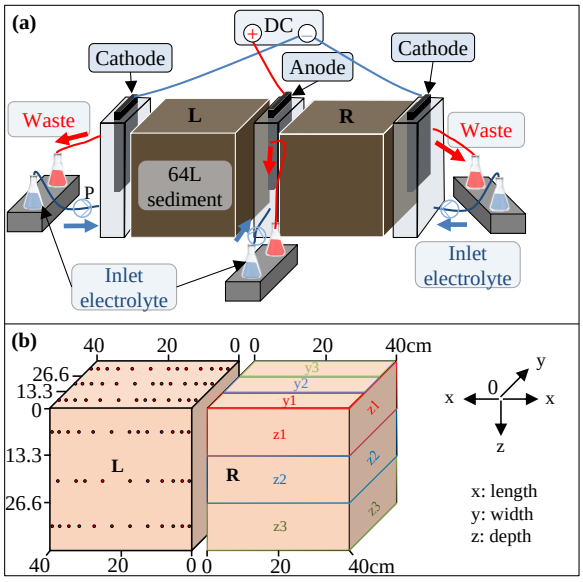

Fig 1 Electrokinetic remediation reactor. a) Schema of the 128 L reactor (L: left compartment, R: right compartment, P: pump). b): The widthwise (y1: 0 – 13.3 cm, y2: 13.3 – 26.6 cm, and y3: 26.6 – 40 cm), and depthwise (z1: 0 – 13.3 cm, z2: 13.3 – 26.6 cm, and z3: 26.6 – 40 cm) segments that were sectioned at the end of the experiment are shown in the "R" compartment; lengthwise (on the x-scale) data acquisition is shown as circular shapes in the "L" compartment

At first, the direct pH and ORP lengthwise and widthwise measurements (y1 – y3) were taken for the surface layer (z1) to study the spatial variation; sediment samples that showed similar physicochemical characteristics along the lengthwise direction (from anode to cathode, x-scale in *Fig 1*b) were grouped and taken as one sample. After the sediments were collected from depth z1, the same strategy was applied to z2 and z3.

2.4. Sediment collection and analyses: physicochemical properties, grain size distribution, and organic and carbonate contents

The fresh sediments that were collected along the lengthwise, widthwise, and depthwise directions were centrifuged for 20 min at 4500 rpm (4640 g or 205 RAD). The electric conductivity and pH of the porewater (PW) were then measured using the same equipment that was used for the measurements in the electrolyte chambers. The sediment samples were then frozen and freeze-dried for later analyses. However, a fresh sample was stored at 4°C for grain size distribution (GSD) analysis. The dried sediments were then ground using an agate mortar and pestle.

Grain size distribution and particle percentiles (D_{10}, D_{50}, and D_{90}) were determined using a Mastersizer 2000 with a Hydro 2000MU dispersion unit (Malvern Instruments); fresh and non-ground sediments were mixed with distilled water and duplicate measurements (each of 60s) were collected for each sample. Afterward, sonication was applied for 60s before another duplicate measurement was collected. Organic matter contents were estimated according to the loss on ignition (LoI) method (Heiri et al. 2001). The sample positioning in the furnace was optimized so that 95% of the results lie within the confidence interval of ± 0.20 standard error of the mean. Carbonate contents were calculated using the volumetric calcimeter method (ISO 10693 1995).

2.5. Statistical analyses

The significance of the spatial variation of the sediments' physicochemical parameters was tested by a general multivariate analysis of variance using IBM SPSS Statistics Version 25.0. The depthwise and widthwise sections were used as fixed factors and the physicochemical parameters were set as variables. Tukey's HSD (honestly significant difference) was run in case the ANOVA models detected significant effects ($P < 0.05$).

2.6. Crystalline mineralogy: X-ray diffraction

The bulk mineralogy of the sediments (initial and after EKR) was characterized by randomly-oriented powder X-ray diffraction (XRD) measurements using PANalytical X'pert with a cobalt monochromatic radiation source (λ CoK_α = 1.78901 Å). Finely ground sediment samples were back-loaded onto 16 mm stainless-steel circular cavity holders and were run in the 5-80° 2θ range using 0.013° step size, 4 s/spin, 40 kV, 40 mA, 0.04 rad Soller slits, 1/8° incident divergence slit, 1/2 mm anti-scattering receiving slit, and a 10 mm mask. The minerals were identified using the HighScore Plus software (Degen et al. 2014) and then quantified from the experimental diffractograms by Rietveld refinement using Profex-BGMN (Post and Bish 1989; Doebelin and Kleeberg 2015; Döbelin 2021) and structural data from the Crystallography Open Database (COD). Oriented mounts were prepared on glass slides (air-dried, treated with ethylene glycol, and calcinated at 550°C) to characterize the clay minerals of the initial sediment using the protocol developed at the Laboratoire Interdisciplinaire des Environnements Continentaux (LIEC), Nancy, France (Poppe et al. 2001; Bihannic and Gley 2021). The results of the oriented mounts are included in *SM 2*.

2.7. Infrared spectroscopy

The organic and chemical signatures of the sediments were identified using Fourier transform infrared spectroscopy (FTIR, Spectrum 3, PerkinElmer Frontier Inc.). The pellets were prepared by pressing 1% of the sample in FTIR grade KBr. For each sample, 8 spectra were collected in the 4000 – 400 cm^{-1} range with a 4 cm^{-1} spectral resolution. The spectra were then normalized by the open-source MCR-ALS GUI (multivariate curve resolution alternating least square gentle user interface) provided by the Vibration Spectroscopy Core Facility at Umeå University (https://www.umu.se/en/research/infrastructure/visp/downloads). The results are included in *SM 3*.

DOI: 10.1007/s11356-023-30271-8
Published in Environmental Science and Pollution Research

Table 1: Initial sediment properties (average ± standard deviations) and mineral composition

				Main crystalline minerals (%)	
pH	7.36	±	0.05	Quartz	24.7
EC (mS/cm)	21.3	±	1.1	Calcite	29.0
ORP (mV)	21.2	±	5.6	Illite	19.1
D_{50} (µm)	14.2	±	0.3	Kaolinite	8.3
Clay particles (%)	5.2	±	0.5	K-feldspars	3.8
Silt particles (%)	87.4	±	1.2	Albite	3.5
Sand particles (%)	7.4	±	0.7	Dolomite	2.9
Water content (%)	62.2	±	2.0	Aragonite	2.5
LoI_{550} or OM (%)	13.3	±	0.3	Smectite	2.0
Carbonates	30.9	±	0.2	Halite	0.5
				Others	3.7

EC: electric conductivity
LoI: loss on ignition
OM: organic matter
ORP: oxidoreduction potential

2.8. Metal quantification: X-Ray fluorescence

The metal contents of the sediments (initial and after treatment) were quantified using X-ray fluorescence spectroscopy (XRF Xepos - AMETEK) at PLATIN' (PLATeau d'Isotopie de Normandie) core facility (Caen, France). Freeze-dried and finely-ground homogeneous sediments were used to quantify major (Al, Ca, Cl, Fe, K, Mg, Mn, Na, P, S, Si, and Ti) and trace (As, Ba, Ce, Co, Cr, Cs, Cu, Ga, Hf, Mo, Nb, Ni, Pb, Rb, Sr, Th, Tl, U, V, W, Y, Zn, and Zr) elements; EnviroMAT SS-1 and EnviroMAT SS-2 were used as certified reference materials. Selected elements are reported in this paper, which are potentially toxic trace elements (Ni, Sr, and Zn) as well as major elements that serve as macro-nutrients for plants (Ca, Mg, and Na).

3. Results

The statistical data (ANOVA and post-hoc Tukey's HSD test, $P < 0.05$, SM 1) showed that there is no significant variation of the physicochemical parameters (i.e., pH and EC) between the compartments (L and R), depths (z1 – z3), and widths (y1 – y3); an exception was the pH of z1 (depth 0 – 13.3 cm), which was significantly different from z2 and z3 (further explanation is included in section *3.3*). The statistical data and more information are included in SM 1. The results indicate that the variation in the EKR reactor was lengthwise (i.e., from anode to cathode). Thus, the results for lengthwise variation are presented below and each of the three widths, three depths, and two compartments were taken as replicates for physicochemical analyses. Based on these results, representative samples were taken for grain size distribution analyses, mineral identification, and organic, carbonate, and metal quantification.

3.1. Temporal evolution of the electrical parameters

The EK experiment started with a 2.4 A current (i.e., 1.2 A or 0.75 mA/cm^2 per compartment) and a 40 V voltage (1 V/cm). Within a few minutes after starting the experiment, the current increased due to a drop in resistance, while the voltage remained stable (inset in *Fig 2*a). The drop in resistance represents an increase in conductivity caused by the production of H^+ and OH^- in the anode and cathode chambers due to water oxidation (*Eq 1*) and reduction (*Eq 2*), respectively. The drop in resistance also indicates the movement of those ions to the oppositely-charged electrodes, thus highlighting the sediment's permeability.

Eq 1 $$2H_2O_{(l)} \rightarrow 4H^+_{(aq)} + O_{2(g)} + 4e^-$$

Eq 2 $$2H_2O_{(l)} + 2e^- \rightarrow 2OH^-_{(aq)} + H_{2(g)}$$

It is also expected that other ions will be released from the sediments. Indeed, the electric parameters depend on ion availability in the electrolyte chambers and the porewater. The highest reachable current in this setting was 5.5 A (i.e., 2.25 A or 1.4 mA/cm^2 per compartment). After that point, the ongoing drop in resistance was followed by a voltage decline. The daily resistance and voltage mainly changed during the first 4 days. However, there was always a difference between the daily starting and final voltages (*Fig 2*b). When the current was constant, the relatively higher daily final voltages are explained by the removal of conductive species from the medium. It is worth noting that the resistance, and consequently the voltage, increased at day 15 (i.e., after 120 hrs of treatment), while the current remained stable. Eventually, a relatively stable medium was reached after day 7, as noted by insignificant changes in electric parameters. This can be due to limited species that were released from the sediments and when H^+ and OH^- fluxes no longer affected the system (i.e., sediment and porewater). Applying a periodic voltage improves the EK process by allowing the ionic species to migrate in the porewater when no electricity is applied (Ammami et al. 2015), i.e., for 16 hrs per day in our case. The migration of those ions is then furthered upon DC application.

DOI: 10.1007/s11356-023-30271-8
Published in Environmental Science and Pollution Research

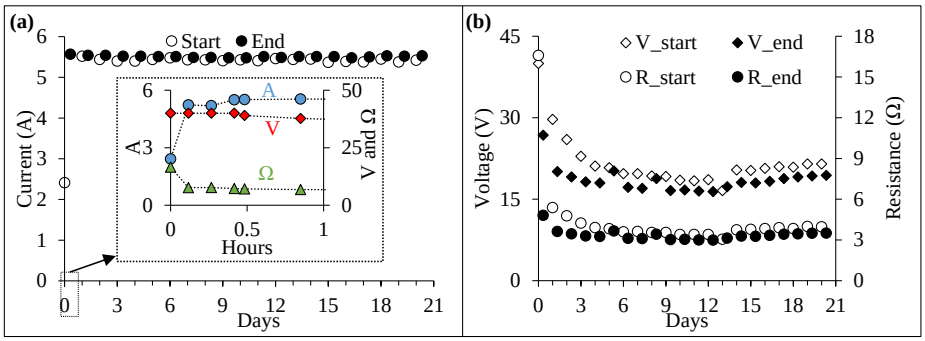

Fig 2 The evolution of a) current (ampere "A") and b) voltage (volt "V") and resistance (Ohm "Ω") as a function of time. The inset in "a" highlights the changes (current, voltage, and resistance) that occurred within an hour of starting the experiment. Values were recorded at the start (daily starting) and end (daily final) of the daily 8 hr current application

3.2. Temporal evolution of temperature, EC, and pH

The physicochemical and electric parameters of the two cathode chambers were similar; therefore, they were taken as replicates and the averages are reported. The EK experiment was run under ambient room temperature. Thus, the daily starting temperatures varied and ranged between 14 and 17°C (*Fig 3*a). The starting temperatures also depended on the final temperatures that were reached at the end of the previous day. The highest temperature was reached at the end of the first day and then gradually decreased with time. The temperature variation is explained by the Joule effect (generation of heat when an electric current passes through a medium). Higher temperatures indicate higher resistance in the medium. The daily decline in the final temperatures is then due to a decrease in resistance (i.e., EC increase in the medium). This is caused by the periodic introduction of H^+ and OH^- in the electrolyte chambers and their mobility toward the oppositely-charged electrodes. This migration is also possible when electricity is not applied (i.e., during 16 hrs daily), as ions will diffuse in the porewater. The transfer of elements from the sediment to the porewater, via release, desorption, or dissolution, also explains the decline in temperature with time. Although those ions move to the oppositely-charged electrodes, it is expected that some of them remain in the system due to pH restraints, such as acid and base fronts (Wen et al. 2021b). During the first two days, the cathode chamber had higher daily final temperatures than the anode. This is explained by the ionic mobility of H^+ (34.9 $mS.m^2.mol^{-1}$) generated in the anode (*Eq 1*) that is higher than that of OH^- (19.8 $mS.m^2.mol^{-1}$) generated in the cathode (*Eq 2*). This, however, does not indicate that species released from sediments do not affect temperature change. In the last ~10 days, the daily final temperatures were higher in the anode chamber. During those days, it is thought that a significant fraction of conductive species migrated toward the cathodic zone. It is worth noting that the increase in temperature favors metal release (Li et al. 2013); additionally, the released metals at the end of the day, and after diffusion in the sediment porewater, might be resorbed when temperatures reach initial conditions (e.g., before applying electricity the following day).

The electric conductivity generally showed an increasing trend in the first 8 days in both electrolyte chambers (*Fig 3*b). The EC of the anode chamber was always higher than that of the cathode chamber, which is mainly explained by the generation of H^+ ions; H^+has higher ionic mobility than OH^-. Furthermore, the ionic mobility of citrate (4.8 $mS.m^2.mol^{-1}$) and other ionic species (e.g., Ca^{2+}, Mg^{2+}, and K^+) are lower than that of OH^- (Vanysek 1993; Wen et al. 2021b). Therefore, the influence of other cations is limited and less significant compared to primarily H^+ and secondly OH^-. During the first 9 days, the daily final EC values were always higher than the starting ones for both electrolyte chambers. This changed after day 9, suggesting that the influence of EK on ionic species release is limited or that the medium has reached a quasi-stable phase.

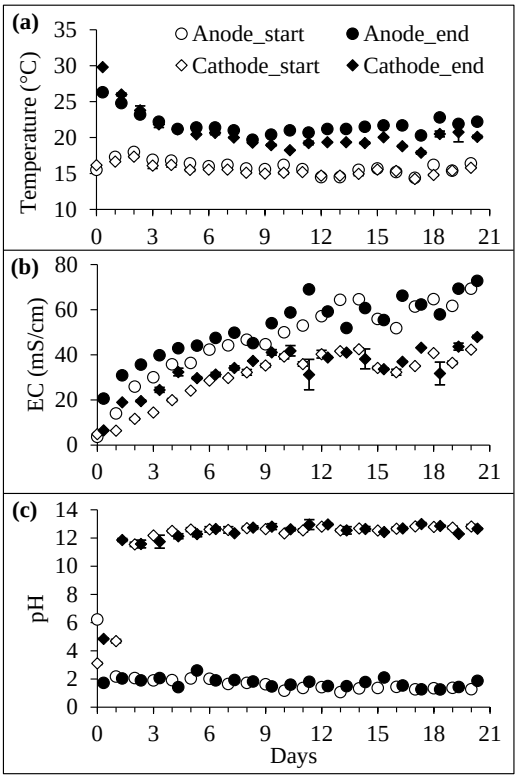

Fig 3 The variation of a) temperature (°C), b) EC (mS/cm), and c) pH of the anode and cathode chambers during treatment. The left and right cathode chambers were taken as replicates and the average values are represented with standard deviations as vertical error bars

The oxidizing and reducing conditions of the anode and cathode chambers, respectively, explain the pH trend (*Fig 3*c). The generation of H^+ in the anode chamber reduced the initial pH in the chamber from 6.2 to 1.7 on the first day. The daily starting pH values then slightly increased to 2.2 and remained almost stable until the end of the experiment. In the cathode chamber, the pH increased from 3.1 to 4.9 on day 1 and then to 11.5 at the end of the second day. Thus, the presence of citric acid (0.1 M) in the cathode chamber

DOI: 10.1007/s11356-023-30271-8
Published in Environmental Science and Pollution Research

was not sufficient to condition the generation of OH^- at the cathode. This value was maintained throughout the 21-day experiment. Except for the first two days, the daily starting and final pH values were similar and did not vary with time.

Due to the continuous reactions in the anode and the cathode chambers during treatment, the ORP values did not stabilize and therefore only represent a rough idea about the redox potential. In general, the ORP values averaged 996±280 mV and 401±317 mV in the anode and cathode chambers, respectively. This parameter affects the chemical and biological reactions that occur in sediments, such as the oxidation of sulfides and the reduction of iron oxides and oxyhydroxides, which in turn affect metal behavior and abundance of species (e.g., Lynch et al. 2014).

3.3. Spatial distribution of pH, ORP, and EC in the sediments

The direct pH measurements in the sediments and the ones measured from the extracted PW showed similar trends. However, the direct pH measurements in the sediments indicate pH values for certain points, while those of the PW represent the average pH values for sections. Therefore, and for accuracy reasons, only the direct pH measurements in the sediments are reported (*Fig 4*a). The pH of the sediments along the anode-cathode direction showed a typical trend (e.g., Ammami et al. 2013; Kim et al. 2013), with highly acidic conditions near the anode (~2) due to H^+ production (*Eq 1*) and highly alkaline conditions near the cathode (~12) due to OH^- production (*Eq 2*). The pH values were different for z1 on the one hand and z2 and z3 on the other in the 12 – 30 cm sediments. This variation might be explained by sediment surface disruption that was unintentionally caused by pH and redox potential measurements that were collected during the first week of the experiment. Therefore, this variation will be considered an artifact and will not be commented on; the z1 layer was not considered for chemical, mineral, and grain size analyses. The pH values of the 0 – 10 cm and 30 – 40 cm sediments were generally lower and higher than the initial pH, respectively. The final pH (8.2) of the combined sediment samples was higher than the initial one (7.4). The final pH was calculated based on the direct measurements that were taken throughout the reactor (i.e., lengthwise, widthwise, and depthwise in the L and R compartments).

The sediments near the anode were oxic due to the oxidation of water and the release of O_2 (*Eq 1*) and the sediments near the cathode were anoxic due to the reducing conditions caused by water reduction (*Eq 2*) (*Fig 4*b). The ORP of the initial sediment was 21±6 mV. Like pH, the ORP showed distinct values in the anodic (0 – 10 cm) and cathodic (30 – 40 cm) zones. The ORP values of the 10 – 30 cm sediments were comparable to the initial sediment. Furthermore, EK has proven to reduce the ORP of sediments (e.g., Ammami et al. 2020). The change in ORP throughout the sediment after treatment affects the mobility and availability of redox-sensitive elements (Lee et al. 2019).

The EC was highest in the anodic sediments (0 – 4 cm; *Fig 4*c). It then gradually decreased and reached the lowest values in the 15 – 32 cm sediments, and then increased in the cathodic zone. Similar to EC behavior in the chambers (section *3.2*), the main cations that are believed to explain this trend are H^+ and OH^- (produced in the anode and cathode chambers, respectively), and secondly other species that are released from the sediments, such as Ca^{2+} and Mg^{2+}. The removal or transport of ionic species is shown in the 10 – 35 cm sediments since the EC values are lower than the initial sediment. This decrease is thought to come from the intermittent application of a DC current, which helps in reducing EC (Micic et al. 2001). The final EC is 15.2 mS/cm, which is ~29% less than the initial sediment. Reduced EC is desirable if the treated product is to be used in agriculture since salinity negatively affects plant growth (Tian et al. 2020; Ferrans et al. 2022).

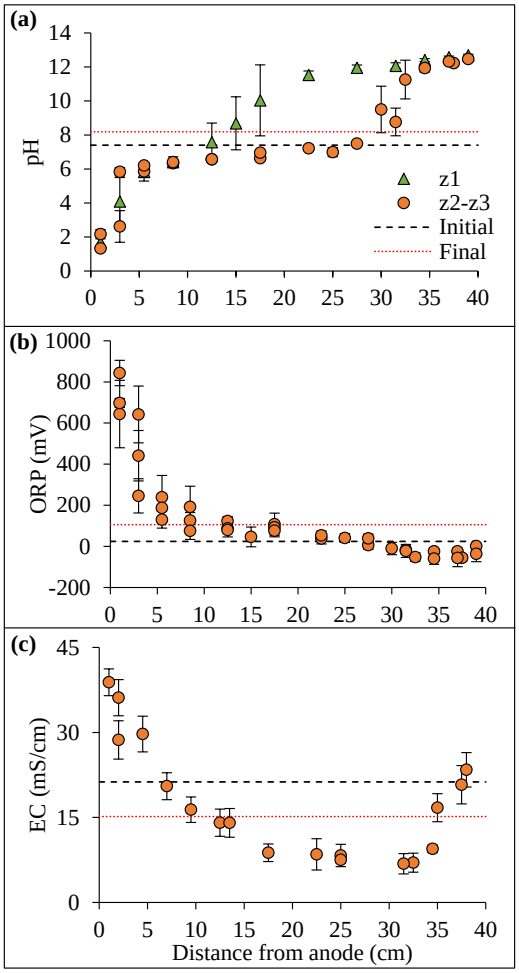

Fig 4 The spatial variation of a) pH, b) ORP (mV), and c) EC (mS/cm) of the sediments at the end of the experiment. The samples at a widthwise scale were taken as replicates (n=3) and are represented as averages with standard deviations as error bars. All the depths were grouped and marked the same, except in the case of pH, which showed that z1 (depth 0 – 13.3 cm) was different from z2 (depth 13.3 – 26.6 cm) and z3 (depth 26.6 – 40 cm)

3.4. Grain size and aggregate properties

The sediments generally showed coarser particles after treatment, as indicated by the shift of the GSD toward larger sizes (*Fig 5*a). The population of the sediments slightly shifted from 23 µm near the anode to 28 µm near the cathode (sonicated samples in *Fig 5*a). Moreover, there were peculiar trends for the different percentiles. For example, the treated sediments had lower D10 values than the initial sediment and decreased in the 30 – 40 cm region. Oppositely, the treated sediments had higher D50 and D90 values than the initial sediment and increased in the 30 – 40 cm region (*Fig 5*b). Finally, there was a significant

DOI: 10.1007/s11356-023-30271-8
Published in Environmental Science and Pollution Research

variation in the GSD upon sonication for the initial sediment (*Fig 5*a), which reflects the aggregation nature of the sediment; this was not detected in the treated sediments, regardless of their position in the EKR reactor.

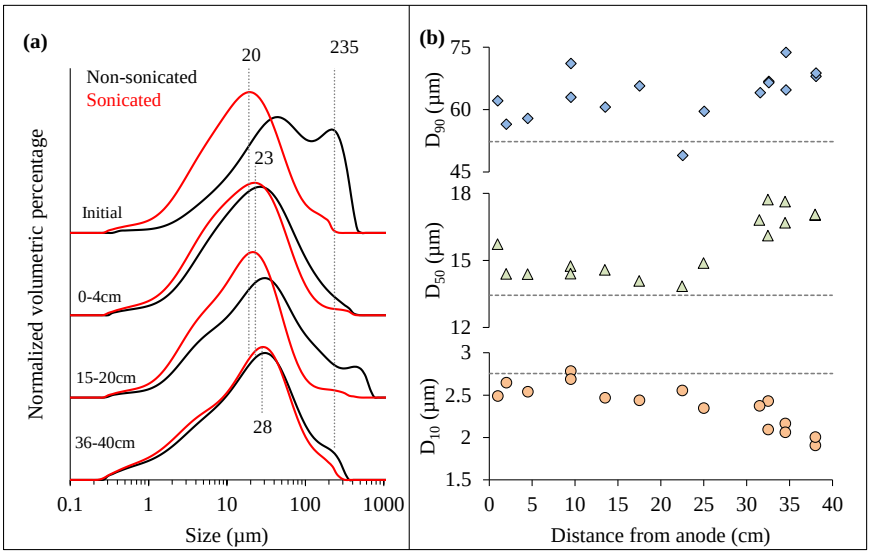

Fig 5 a) Grain size distribution of the initial and treated sediments; the black and red curves indicate non-sonicated and sonicated samples, respectively. b) The percentiles (D_{10}, D_{50}, and D_{90}) of the treated sediments as a function of distance from the anode in comparison to the initial sediment (dashed line)

3.5. Mineral and organic contents

The initial sediment mainly contains silicate minerals, such as quartz, amphiboles (inosilicates), feldspars (tectosilicates), clay minerals (phyllosilicates), and carbonates (calcite, aragonite, and dolomite). More information about clay mineral identification is discussed in *SM 2* (oriented XRD mounts). Among the detected minerals, only carbonates were affected by EK, namely calcite, dolomite, and aragonite (*Fig 6*a). The carbonate contents in the 0 – 4 cm sediments were lower than 4% (*Fig 6*b), while the initial sediment was rich in carbonate (~31%, *Table 1*). This decrease is due to the acidic conditions that dissolved carbonates, which is furthered by the rise in temperature in the anodic sediments (Alkhaldi et al. 2010). The carbonates in the 0 – 4 cm sediments were mainly dissolved, while those of the 10 – 40 cm sediments were comparable to the initial sediment (*Fig 6*a and b). The reduction of carbonate content was also witnessed by infrared spectroscopy (*SM 3*); however, XRD was used to distinguish between calcite, aragonite, and dolomite. The peak intensities of these carbonates were relatively low in the anodic sediment (*Fig 6*a inset). The calcite peak (3.03 Å) significantly decreased and the dolomite and aragonite peaks (2.88 and 3.39 Å) almost disappeared in the 0 – 4 cm sediment (*Fig 6*a). Furthermore, dolomite was weakly detected in the 15 – 20 cm sediment, while calcite was more prominent and similar to the initial sediment. As for the organic matter contents, they were higher in the 0 – 4 cm region in comparison to the initial sediment. The organic matter percentage did not increase, rather it is an overestimation due to carbonate dissolution (~25% mass loss). Nonetheless, the introduction of oxygen in the anode chamber due to water oxidation might promote organic matter dissolution through chemical degradation. Indeed, the rate of chemical degradation of OM under oxic conditions (in the anodic zone) is faster than in anoxic conditions (Kristensen et al. 1995). Finally, the 20 – 40 cm sediments showed slightly lower OM than the initial sediment.

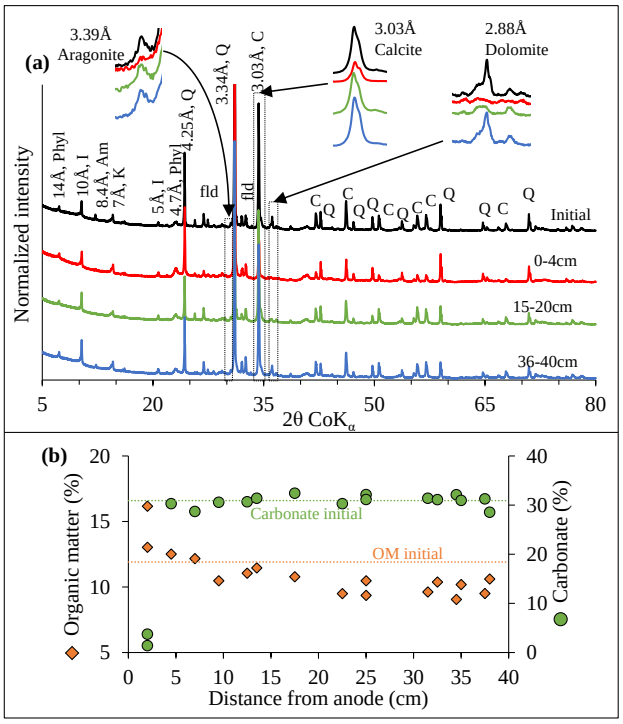

Fig 6 Spatial variation of a) crystalline minerals (XRD) and b) carbonate and organic matter contents (the initial contents are plotted as dashed lines for comparison purposes). Phyl: phyllosilicates (more information about the phyllosilicate minerals is included in *SM 2*), I: illite, Am: amphibole, K: kaolinite, Q: quartz, C: calcite, and fld: feldspars. The insets highlight the dissolution of carbonate minerals in the 0 – 4 cm sediment

3.6. Behavior of major and trace elements

The metal removal percentage is not reported per section due to the loss of carbonates in the anodic sediments; this will overestimate metal loss by up to 30% (similar to OM overestimation, section *3.5*). Anyway, Na and Mg were significantly removed from the sediments, especially in the anodic zone (*Fig 7* a, b). This is due to their cationic nature that facilitates their mobility toward the cathodic zone. The possible elemental species (Na, Mg, and other elements that are later presented in the text) as a function of pH are

DOI: 10.1007/s11356-023-30271-8
Published in Environmental Science and Pollution Research

included in *SM 4* (using Visual MINTEQ, version 3.1). However, the Na and Mg trends were dissimilar; the boundary where the metal content is higher than the initial content is ~30 cm for Na and ~20 cm for Mg. This indicates higher mobility for Na over Mg since monovalent Na has a lower affinity to sediment components than divalent Mg (Klitzke and Lang 2009).

Similar to Mg and Na, Ca and Sr are found as positive species regardless of pH (*SM 4*). Calcium content was relatively lower in the anodic sediments (*Fig 7*c). This indicates that most Ca is held within carbonate species that dissolved in acidic conditions (section *3.5*). The same applies to Mg due to dolomite ($CaMg(CO_3)_2$) dissolution (*Fig 6*a inset). The XRD data showed that dolomite dissolution occurred farther away from the anode than calcite (the dolomite peak was absent in the 15 – 20 cm sediment). Despite this, Ca did not fluctuate much in the 5 – 40 cm sediments, probably because dolomite content is significantly lower than calcite (*Table 1*). The similar behavior between Sr and Ca suggests that Sr is mainly found in carbonate minerals (*Fig 7*c and d).

Nickel content was successfully reduced from the sediments throughout the EK reactor (*Fig 7*e). Nickel is mainly found as cationic species when pH is below 9 and as aqueous and anionic species between 9 – 11 and above 11, respectively. The Ni contents ranged between 50 and 63 mg/kg after treatment, while it initially was 74 mg/kg. Thus, the removal ranged between 14% and 28%. There was no clear trend for Ni as a function of distance from the anode electrode. Zinc content was also reduced after treatment except for limited regions near the anode (0 – 2 cm sediments, *Fig 7*f). Higher Zn contents in the anodic sediment can be an overestimation due to carbonate dissolution (as mentioned previously). However, the removal percentage ranged between 8% and 34%.

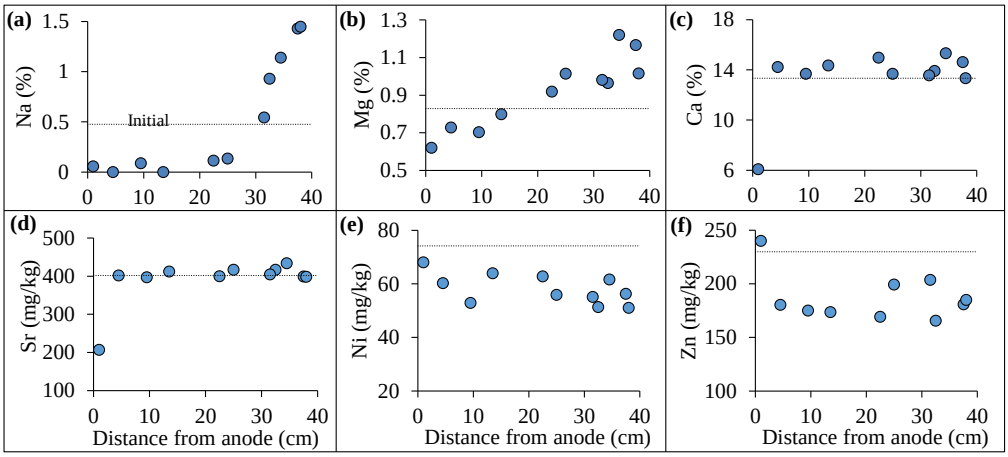

Fig 7 The variation of a) Na (%), b) Mg (%), c) Ca (%), d) Sr (mg/kg), e) Ni (mg/kg), and f) Zn (mg/kg) in the sediments after treatment. The dotted lines represent the initial metal contents

3.7. Electric consumption

The daily energy consumption decreased with time due to the drop in voltage while the current remained stable. The almost instant drop in resistance was caused by the introduction of ionic species in the porewater (as described in section *3.1*). After approximately 14 days of decrease in the daily energy consumption, it unexpectedly increased during the last 5 days (*Fig 8*). Energy consumption depends on the type of matrix, treatment time, composition, and chemical species (e.g., Zhou et al. 2006). In the case of estuarine sediments, or other media with high conductivity (*Table 1*), the conductive species improved the transmittance of current while maintaining a relatively low voltage gradient; this was the case in the first hours of the experiment (*Fig 2*). This in turn enhances metal release without having to increase power consumption. In total, the energy consumption was 140 KWh/m^3 or 0.117 KWh/Kg for the 128 L reactor, which is similar to the values reported by other studies with comparable running times (e.g., Zhou et al. 2006).

4. Discussion

4.1. Physicochemical and electric parameters reveal processes that occur in EK over time

The parameters that were monitored during EK remediation displayed a specific pattern during the initial 8 days (i.e., 64 hrs of electric current application). This was mainly seen by the gradual drop in voltage and temperature (*Fig 2*b and *Fig 3*a) as well as the drop in the difference between the daily final and starting values of these parameters (ΔV and ΔT, *Fig 9*a). The gradual decrease in voltage and ΔV under constant current is explained by a reduction in resistance, or an increase in ionic species or EC. Media with lower conductivity can transmit more heat (Kaviany 1995). Therefore, the significant ΔT values during the first few days are explained by the removal of conductive species from the sediments. Moreover, ΔT was higher for the cathode chamber during the first 6 days, while it was reversed for the later days (*Fig 9*a). The ΔT variations in the anode chamber were greater in the latter period due to more drastic EC variations (*Fig 9*b).

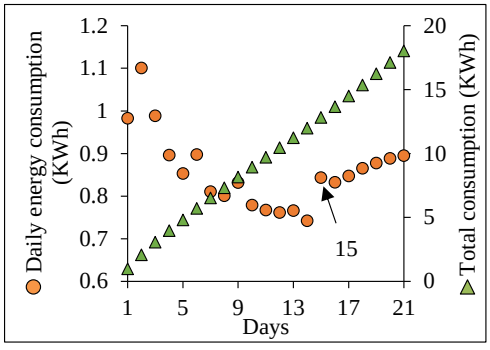

Fig 8 Daily and total energy consumption during treatment (KWh)

The ΔT increase after days 10 and 12 in the anode and cathode chambers, respectively, suggests that the medium was not as stable as it was between days 4 and 7 (*Fig 9*a).

DOI: 10.1007/s11356-023-30271-8
Published in Environmental Science and Pollution Research

Indeed, EC showed a peculiar increasing trend after day 8 (*Fig 3*b); this increase was not detected by voltage or current (*Fig 2*). However, the variation in ΔEC, specifically after day 8, suggests that precipitation and dissolution reactions occurred in the sediment and/or porewater. Indeed, these EC values largely fluctuated in comparison to the first 7 days (*Fig 3*b and *Fig 9*b). Based on the sediment composition and pH, calcite (*Eq 3*) and dolomite (*Eq 4*) are possibly dissolved and precipitated in the anode and cathode regions, respectively (López-Vizcaíno et al. 2019).

Eq 3 $CaCO_{3(s)} \leftrightarrows Ca^{2+}_{(aq)} + CO^{2-}_{3(aq)}$

Eq 4 $CaMg(CO_3)_{2(s)} \leftrightarrows Ca^{2+}_{(aq)} + Mg^{2+}_{(aq)} + 2CO^{2-}_{3(aq)}$

The EC and temperature were strongly and negatively correlated during the first 7 days (*Fig 9*c). This correlation, although to a lesser extent, persisted in the cathode chamber until the end of the 21 days (*Fig 9*c). The lack of correlation between the mentioned parameters in the anode region is likely attributed to further reactions taking place, specifically the dissolution of calcite (*Eq 5*) and, to a lesser extent, dolomite (*Eq 6*) caused by the acidic conditions.

Eq 5 $CaCO_{3(s)} + 2H^{+}_{(aq)} \rightarrow Ca^{2+}_{(aq)} + CO_{2(g)} + H_2O_{(l)}$

Eq 6 $CaMg(CO_3)_{2(s)} + 4H^{+}_{(aq)} \rightarrow Ca^{2+}_{(aq)} + Mg^{2+}_{(aq)} + 2CO_{2(g)} + 2H_2O_{(l)}$

The pH in the anode and cathode chambers reached a quasi-stable stage as early as day 3 (*Fig 3*c). The change in pH commonly occurs within a few hours of current application (e.g., Xu et al. 2022). Furthermore, the anode chamber reached a stable pH faster than the cathode chamber (e.g., Liu et al. 2023). In our case, this can be explained by the presence of citric acid in the cathode chamber that buffered the increase in pH until the end of the second day. When compared to non-acidic electrolytes (e.g., KCl and ultra-pure water), citric acid delayed pH increase and the time to reach a stable pH (Wu et al. 2016). As for the anode, the pH decline can be delayed by carbonate dissolution. The significant decrease in pH, despite the high carbonate contents of the initial sediment (*Table 1*), indicates that carbonate dissolution (*Eq 5* and *Eq 6*) did not have a considerable effect on buffering the anode medium. However, the buffering capacity should be more prominent in the porewater (i.e., sediment compartment) than in the anode chamber.

Based on the physicochemical (pH, EC, and T) and electric (voltage and current) parameters of the chambers that were daily collected, three clusters were distinguished, which are 1 – 7, 8 – 14, and 15 – 21 days (*Fig 9*d). The first and third phases were characterized by negative and positive PC1 (principal component) loadings, respectively. The first phase included the increase of conductive species in the porewater, as reflected by EC increase (*Fig 3*b) and consequent changes in electric parameters (as discussed in sections *3.1* and *3.2*). The second phase marked a relatively constant phase where those parameters remained quasi-stable (PC1 loadings near zero). The third phase was identified by a peculiar increase in EC, T, ΔT, and I, as well as a notable increase in energy consumption (day 15, *Fig 8*). Those changes are strongly thought to be caused by further carbonate dissolution that consequently reduced the buffering capacity. As a result, the acidic front of the sediment advanced which in turn affects the speciation and mobility of elements (e.g., Carrillo-González et al. 2006; López-Vizcaíno et al. 2019). It should be noted that positive and negative loadings of PC-2 mark the daily starting and final values, respectively (*Fig 9*d). The grouping of the parameters as a function of day can be used to suggest adequate treatment time. Initially, it seemed that 8 days were sufficient to reach a stable medium and thus ending the experiment; i.e., applying an electric current for 64 hrs. Indeed, some studies showed that equilibrium was reached after applying an electric current for 64 – 100 hrs (e.g., Lu et al. 2012; Zein-Eddin et al. 2023). During 192 hrs of surveillance, Lu et al. (2012) claimed that ion migration was retarded after 96 hours of electric current application, thus suggesting that 96 hrs were sufficient for effective metal remediation in their case. However, the period of treatment depends on the composition of the treated material as well as the running parameters (e.g., López-Vizcaíno et al. 2019; Han et al. 2021). Therefore, the treatment period is case specific. In our case, the sediments showed a peculiar behavior after a ~5-day quasi-stable period. This highlights the importance of characterizing the initial material on the one hand and monitoring and understanding the variation of physicochemical and electric parameters during EK on the other. For example, metal behavior is largely dependent on pH, which in turn depends on the processes that happen in the sediment's porewater and anode and cathode chambers. Indeed, metals are generally more mobile under acidic conditions due to the formation of metal ionic species, competition with H^+, and alteration of surface charge (e.g., Carrillo-González et al. 2006; Du Laing et al. 2009).

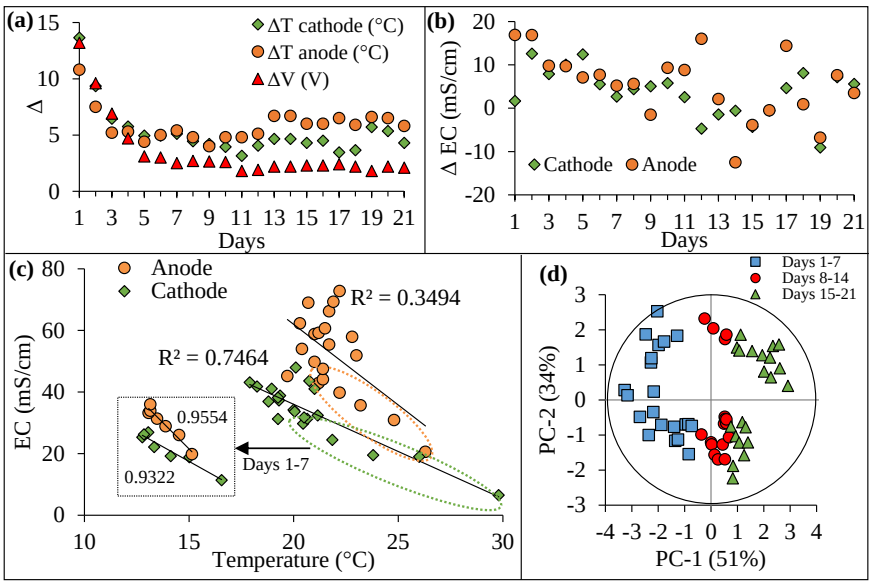

Fig 9 The variation of a) ΔV (V) and ΔT (°C), b) ΔEC (Δ: the difference between the daily final and starting values), and c) the correlation between temperature and EC for the anode and cathode chambers as a function of time. d) Principal component analysis (PCA) matrix for the physicochemical and electric data (daily starting and final values) that were collected during the experiment

DOI: 10.1007/s11356-023-30271-8
Published in Environmental Science and Pollution Research

4.2. Processes in sediments and link to metal behavior

The sediment's depthwise homogeneity was mainly verified by EC and pH, and secondly by mineral, organic, and metal contents (*SM 1*); an exception was the pH of the surface layer (z1), as discussed in section *3.3*. Thus, the effect of compaction on EK in this reactor is excluded, especially in the deepest layer (z3). The continuous generation of H^+ (*Eq 1*) and OH^- (*Eq 2*) in the anode and cathode chambers, respectively, explain the high EC in the anodic and cathodic sediments (*Fig 4*c). However, the EC values of the 8 – 35 cm sediments were lower than the initial sediment, thus indicating that ions and/or molecules were transported through the porewater throughout the EK reactor; this process is furthered by the application of an intermittent current (Micic et al. 2001; Xu et al. 2022). This indicates that the sediment's permeability was sufficient for efficient remediation, despite its fine texture (*Table 1*). This opens the question for other possible treatment techniques (e.g., phytoremediation, chemical extraction, flotation, and washing) since the limitations of permeability might not apply here (e.g., Zhang et al. 2021). Nonetheless, EKR is a relatively fast technique that can be applied in-situ (Han et al. 2021; Sun et al. 2023). The possibility of enhancing EKR during treatment is another aspect that makes it a desirable method, such as conditioning pH for selective elemental reduction, changing electrode position to increase metal mobility, and adding surfactants to promote separation of ions or complex free ions (Wang et al. 2021; Sun et al. 2023).

Electroosmosis and electromigration are the dominant drivers for metal transport in EKR (Han et al. 2021 and references therein). The same cannot be said about particle movement or electrophoresis due to the fine texture of the sediment. Moreover, a big part of the EC in the sediment's porewater and anode and cathode chambers are thought to originate from salts that are naturally present in estuarine and marine sediments (e.g., Micic et al. 2001). Indeed, the sediment contains salts (halite, *Table 1*) and is Cl-rich (~6.8%). Additionally, Cl in the porewater can form metal complexes (chloro-complexation), which in turn improves metal mobility (Acosta et al. 2011). The application of EK removes salts due to their cationic nature. This was seen by the reduction of Mg and Na in the anodic sediments (*Fig 7*a and b). It is worth noting that the removal or reduction of salts and trace metals is part of the aims since the treated sediments will be used in agriculture (Interreg ReCon Soil 2022).

Most treated sediments had pH values either above (>30 cm) or below (<30 cm) the initial sediment. This indicates that all the sediments were affected by EK. The predominant citric acid species in most 0 – 2 cm sediments was H_3citrate (*Fig 10*b). The predominant species then became H_2citrate$^-$ and H citrate^{2-} in the 2 – 7 cm sediments and finally citrate^{3-} for the remaining sediments (10 – 40 cm, Visual MINTEQ, version 3.1). This shows that citric acid functioned as an efficient sorbent throughout the EK reactor, except the nearest 2 cm from the anode. Additionally, the added citric acid in the cathode chambers, as citrate^{3-} species, will migrate toward the anode due to the difference in charge. The 0 – 2 cm sediments will have neutral citric acid species and therefore metal ions cannot form complexes with citric acid. Instead, metals will migrate via the difference in charge when the current is applied (i.e., 8 hrs per day) and by diffusion when there is no current (i.e., 16 hrs per day). Otherwise, metals will not be reduced from said regions. Indeed, the treated sediments had lower Zn contents than the initial sediment except in the 0 – 2 cm region (*Fig 7*f).

Acidic and basic fronts are created by water oxidation and reduction in the anode and cathode chambers, respectively. This leads to the generation and enrichment of H^+ and OH^- in sediments that are in contact with the chambers. Indeed, relatively high EC values in the anodic and cathodic sediments indicate H^+ and OH^- accumulation. The ionic mobility of H^+ and OH^- are 36.2 and 20.5 $m^2/s/V$, respectively. The pH alteration extended until 4 cm in the anode region and ~10 cm in the cathode region. The pH alteration in the cathode region is usually more significant than that of the anode (e.g., Xu et al. 2022). Furthermore, our sediment was rich in carbonates (31%, *Table 1*), which makes it a strong buffering medium and can reduce the advancement of the acidic front. López-Vizcaíno et al. (2019) showed that higher calcite (carbonate) contents in a modeled soil reduced the advancement of the acidic front; López-Vizcaíno et al. (2017) showed that the buffering system of carbonates affected the spatial evolution of pH. After EKR, the buffering capacity of the anodic sediments decreased due to carbonate dissolution (*Fig 6*b), which further affect metal mobility and transport (Roberts et al. 2005; Carrillo-González et al. 2006). Another indication of carbonate dissolution is the variation in physicochemical and electric parameters during the start of phase 3 (*Fig 9*d). Unfortunately, the sediment's pH was not monitored during the experiment to avoid disturbing the surface and thus disrupting the homogeneity of the medium. Nonetheless, carbonate dissolution is expected to have started during phase 1, right after the acidic front formed. This front then advanced and resulted in progressive carbonate dissolution. Due to the relatively stable conditions during phase 2, it is thought that the carbonate dissolution rate decreased and continued in phase 3. Cai et al. (2021) showed similar observations when the current increased upon electrolyte (lactic acid) addition. They related EC increase to the electrolyte itself as well as the dissolution of acid-soluble fractions in the soil. The dissolution of salts and carbonates increases ionic strength and therefore enhances metal release through metal exchange processes, which is metal and species-dependent (e.g., Du Laing et al. 2008, 2009; Kanbar et al. 2018).

An increase in temperature, especially in the first few days (*Fig 3*a), and the introduction of H^+ promote carbonate dissolution (*Eq 5* and *Eq 6*) (e.g., Alkhaldi et al. 2010). Consequently, and in the presence of sulfates, the released Ca^{2+} can precipitate to form gypsum, or other calcium sulfate minerals (Van Driessche et al. 2019). Gypsum precipitation was also evidenced in the same sediment under different running conditions (Kanbar et al., in progress). Gypsum precipitation is promoted by the presence of sulfates and Ca ions (that originate from carbonate dissolution, *Eq 3* – *Eq 6*) and occurs under relatively low temperatures (between 25 – 90°C) when the pH ranges between 2 and 3 and (Xu et al. 2019).

Carbonic acid (H_2CO_3) is formed in the anode chamber and the porewater of the 0 – 4 cm sediments due to the acidic conditions (pH<4.3; *Eq 7*). In the 4 - 27 cm sediments where the pH roughly ranges between 4.3 and 8.2, carbonic acid dissociates into bicarbonate ions (HCO_3^-) by releasing H^+

DOI: 10.1007/s11356-023-30271-8
Published in Environmental Science and Pollution Research

(*Eq 8*). Furthermore, and when the pH is above 8.2, bicarbonate ions further dissociate to release H^+ and carbonate ions (CO_3^{2-}) (*Eq 9*).

Eq 7 $CO_{2(aq)} + H_2O_{(l)} \leftrightarrows H_2CO_{3(aq)}$; pH<4.3

Eq 8 $H_2CO_{3(aq)} \leftrightarrows HCO^-_{3(aq)} + H^+_{(aq)}$; 4.3<pH<8.2

Eq 9 $HCO^-_{3(aq)} \leftrightarrows CO^{2-}_{3\,(aq)} + H^+_{(aq)}$; pH>8.2

However, dissolved carbonates can then precipitate in the sediments by reacting with bicarbonate ions when the pH is between 4.3 and 8.2 (*Eq 8* and *Eq 10*) or with carbonate ions when the pH is above 8.2 (*Eq 3*).

Eq 10 $2HCO^-_{3(aq)} + Ca^{2+}_{(aq)} \leftrightarrows CaCO_{3(s)} + H_2O_{(l)} + CO_{2(g)}$

Other ions, such as monovalent (e.g., Na^+ and K^+) and bivalent (e.g., Mg^{2+}, Zn^{2+}, and Pb^{2+}) cations, also form complexes with bicarbonate and carbonate ions (Wierzba et al. 2022; Yan et al. 2022). For example, poorly soluble metal carbonates can form when pH is above 8.2 by reacting with carbonate ions (*Eq 11* and *Eq 12*). Additionally, monovalent (*Eq 13*) and bivalent (*Eq 14*) cations can react with hydroxide ions that are produced from water reduction (*Eq 2*) and precipitate (*Eq 13* and *Eq 14*) in the cathodic zone (Yan et al. 2022).

Eq 11 Monovalent $2M^+_{(aq)} + CO^{2-}_{3\,(aq)} \rightarrow M_2CO_{3(s)}$

Eq 12 Bivalent $M^{2+}_{(aq)} + CO^{2-}_{3\,(aq)} \rightarrow MCO_{3(s)}$

Eq 13 Monovalent $M^+_{(aq)} + OH^-_{(aq)} \rightarrow MOH_{(s)}$

Eq 14 Bivalent $M^{2+}_{(aq)} + 2OH^-_{(aq)} \rightarrow M(OH)_{2(s)}$

The alkaline pH in the cathodic sediments (mainly 30 – 40 cm) can dissolve OM and the acidic conditions in the anode region (mainly 0 – 4 cm) can dissolve carbonates (*Fig 4*a). Since those compounds act as cementing materials, their removal can reduce their aggregation capacity, which was seen by GSD (*Fig 5*a). Furthermore, acidic conditions can disaggregate organo-mineral complexes (e.g., Li et al. 2018), as indicated by the difference between the sonicated and non-sonicated GSD, regardless of the position within the EKR reactor (*Fig 5*a).

Two components explained metal behavior upon EKR. The first explained 59% of the variance and is linked to carbonate dissolution. The second explained 16% of the variance and is linked to pH fluctuation (*Fig 10*a). Although pH and carbonate dissolution were strongly linked, metals were correlated to these factors differently. As major and relatively labile elements, Na and Mg were strongly and positively linked to pH (*Fig 10*a). The accumulation of Na and Mg in the cathodic sediments might be caused by the precipitation of hydroxide complexes (*Eq 13*, *Eq 14*, and *SM 4*). As for Ca and Sr, they were linked to carbonate dissolution, which was most prominent in the anodic sediments; Sr is predominantly found in carbonate minerals, such as calcite, dolomite, and aragonite (Brand et al. 1998). Moreover, the dissolution of calcite, aragonite, and dolomite (*Fig 6*a and b) and consequent Ca and Mg release boost the desorption of surface-bound metals. Indeed, H^+, Ca^{2+}, and Mg^{2+} can displace exchangeable metals (e.g., Carrillo-González et al. 2006; Ayyanar and Thatikonda 2021). Although carbonate dissolution is pH dependent, they were only directly linked in sediments with pH values lower than 4, i.e., in the 0 – 4 cm sediments. As for Zn and Ni, they were less dependent on pH and not related to carbonate dissolution; Zn and Ni have a strong affinity to minerals, such as oxides and oxyhydroxides (e.g., Miranda et al. 2021). Finally, it was shown that Mg, Ca, and Sr were redistributed in the EK reactor, while Na, Ni, and Zn were reduced by 25%, 21%, and 19%, respectively. Although these reduction percentages might seem low, especially when compared to metal reduction in spiked matrices (e.g., Reddy and Chinthamreddy 1999; Ghobadi et al. 2021), these values are significant since metals are part of silicate minerals and cannot easily be extracted or removed (e.g., Deer et al. 2013). The reduction percentage depends on the physicochemical conditions of the matrix as well as the speciation form. For example, Zn can be incorporated in silicate minerals as well as in carbonates; Zn in the latter is more mobile and therefore easier to be removed (Deer et al. 2013; Mertens and Smolders 2013). Nevertheless, the treated sediment is not a homogeneous matrix, rather specific sections within the reactor can be used based on the intended use. Indeed, EKR can narrow the enrichment of some metals to certain regions (e.g., Ortiz-Soto et al. 2023). In our case, the 0 – 4 cm sediment would be treated differently than the other sections since the former is enriched in Zn (*Fig 7*d) and lost its buffering capacity (*Fig 6*). The use of other sections of the treated sediments then depends on the acceptable limits for reuse (e.g., amendment in agriculture). The 30 – 40 cm sediments have lower Ni and Zn contents and are more concentrated with macro-nutrients (Ca and Mg) after EKR (*Fig 7*), which make these sediments potentially useful for agricultural use; nonetheless, the 35 – 40 cm sediments have relatively high EC (*Fig 4*c) and therefore can be detrimental to plants (Ferrans et al. 2022).

5. Conclusion

Three phases were detected during sediment treatment by EKR, mainly represented by an increase in ionic strength and therefore metal release (1 – 7 days), a relatively stable phase (8 – 14 days), and carbonate dissolution (15 – 21 days). Metal behavior was mainly linked to the pH of the sediments and secondly to the dissolution of carbonates. Moreover, statistical approaches were used to highlight the

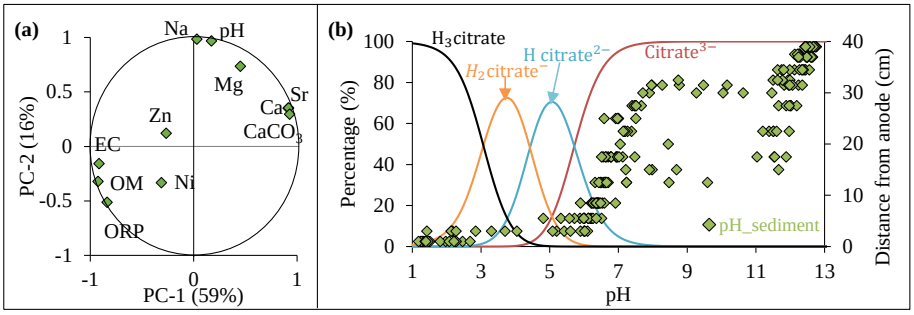

Fig 10 a) Principal component analysis (PCA) matrix for the metal contents, carbonates ($CaCO_3$), organic matter (OM), and physicochemical characteristics (pH, ORP, and EC) of the sediments after treatment. b) The possible citric acid species and pH of sediments (after treatment) as per distance from the anode

importance of monitoring physicochemical data during treatment as well as sediment characteristics after EK. Such information is necessary in EKs especially in materials with high carbonate contents or high buffering capacity. Subsequently, the period of treatment could have been adjusted based on the needed outcome or limitations. The results showed that Na, Mg, Sr, and Ca were only redistributed in the sediments, while Ni and Zn were reduced by 21% and 19%, respectively. The treated sediment overall had lower metal contents and EC (or salinity), which preliminarily show good indications toward using this material in agriculture. Finally, it is essential firstly to characterize the material to be treated (estuarine sediment in this case), understand the reactions and processes that occur upon EKs, and proceed with the treatment accordingly to eventually generate the desired end product. It is also important to minimize any unintended consequences or reaching limitations, such as metal accumulation in unwanted sections or total carbonate dissolution that could reduce the buffering capacity of the medium. Indeed, such an approach assists in reaching environmentally sustainable decisions for polluted or contaminated materials. We will utilize the treated sediments to reconstruct soils to grow zucchini.

Acknowledgment

The authors acknowledge Dr. Benoît Duchemin (LOMC, Le Havre University) and Dr. Nicolas Hucher (URCOM, Le Havre University) for valuable help in running XRD and FTIR measurements. We are most grateful to PLATIN' (Plateau d'Isotopie de Normandie) core facility for all element analysis used in this study. We also thank three anonymous reviewers for their critical review and constructive comments that improved the quality of this work.

Author contribution

Ahmed Benamar, Mohamed-Tahar Ammami, and Hussein J. Kanbar designed the experiment; Hussein J. Kanbar, Mohamed-Tahar Ammami, and Ahmad Zein-Eddin performed laboratory work; Hussein J. Kanbar led the treating of data and writing the paper; all the authors contributed critically to the drafts and gave final approval for publication.

Funding

This work was funded by the European Regional Development Fund (ERDF), Interreg France (Channel Manche) England, ReCon Soil.

Consent to Participate

All authors consent to have participated in the research project that is presented in this paper.

Consent to Publish

The publication has been approved by all co-authors.

Competing Interest

The authors have no relevant financial or non-financial interests to disclose.

Availability of data and materials

Data is available upon request.

References

Acar YB, Alshawabkeh AN (1993) Principles of electrokinetic remediation. Environ Sci Technol 27:2638–2647. https://doi.org/10.1021/es00049a002

Acosta JA, Jansen B, Kalbitz K, et al (2011) Salinity increases mobility of heavy metals in soils. Chemosphere 85:1318–1324. https://doi.org/10.1016/j.chemosphere.2011.07.046

Alkhaldi MH, Nasr-El-Din HA, Sarma H (2010) Kinetics of the reaction of citric acid with calcite. SPE J 15:704–713. https://doi.org/10.2118/118724-PA

Altaee A, Smith R, Mikhalovsky S (2008) The feasibility of decontamination of reduced saline sediments from copper using the electrokinetic process. J Environ Manage 88:1611–1618. https://doi.org/10.1016/j.jenvman.2007.08.008

Ammami M, Benamar A, Wang H, et al (2013) Simultaneous electrokinetic removal of polycyclic aromatic hydrocarbons and metals from a sediment using mixed enhancing agents. Int J Environ Sci Technol 11:1801–1816. https://doi.org/10.1007/s13762-013-0395-9

Ammami M, Song Y, Benamar A, et al (2020) Electro-dewatering of dredged sediments by combined effects of mechanical and electrical processes: Influence of operating conditions. Electrochim Acta 353:136462. https://doi.org/10.1016/j.electacta.2020.136462

Ammami MT, Benamar A, Portet-Koltalo F (2022) Enhanced electroremediation of metals from dredged marine sediment under periodic voltage using EDDS and citric acid. J Mar Sci Eng 10:553. https://doi.org/10.3390/jmse10040553

Ammami MT, Portet-Koltalo F, Benamar A, et al (2015) Application of biosurfactants and periodic voltage gradient for enhanced electrokinetic remediation of metals and PAHs in dredged marine sediments. Chemosphere 125:1–8. https://doi.org/10.1016/j.chemosphere.2014.12.087

Apitz SE (2010) Waste or resource? Classifying and scoring dredged material management strategies in terms of the waste hierarchy. J Soils Sediments 10:1657–1668. https://doi.org/10.1007/s11368-010-0300-9

Ayyanar A, Thatikonda S (2021) Experimental and numerical studies on remediation of mixed metal-contaminated sediments by electrokinetics focusing on fractionation changes. Environ Monit Assess 193:316. https://doi.org/10.1007/s10661-021-09064-4

Benamar A, Ammami M, Song Y, Portet-Koltalo F (2020) Scale-up of electrokinetic process for dredged sediments remediation. Electrochim Acta 352:136488. https://doi.org/10.1016/j.electacta.2020.136488

Benamar A, Tian Y, Portet-Koltalo F, et al (2019) Enhanced electrokinetic remediation of multi-contaminated dredged sediments and induced effect on their toxicity. Chemosphere 228:744–755. https://doi.org/10.1016/j.chemosphere.2019.04.063

Bihannic I, Gley R (2021) Diffraction des rayons X sur

poudres. https://liec.univ-lorraine.fr/content/fiche-diffraction-rayons-x. Accessed 26 Mar 2021

Bose BP, Dhar M (2022) Dredged sediments are one of the valuable resources : A review. Int J Earth Sci Knowl Appl 4:324–331

Brand U, Morrison JO, Campbell IT (1998) Strontium in sedimentary rocks. In: Geochemistry. Kluwer Academic Publishers, Dordrecht, pp 600–603

Butler BA (2009) Effect of pH, ionic strength, dissolved organic carbon, time, and particle size on metals release from mine drainage impacted streambed sediments. Water Res 43:1392–1402. https://doi.org/10.1016/j.watres.2008.12.009

Cai Z, Sun Y, Deng Y, et al (2021) In situ electrokinetic (EK) remediation of the total and plant available cadmium (Cd) in paddy agricultural soil using low voltage gradients at pilot and full scales. Sci Total Environ 785:147277. https://doi.org/10.1016/j.scitotenv.2021.147277

Carrillo-González R, Šimůnek J, Sauvé S, Adriano DC (2006) Mechanisms and pathways of trace element mobility in soils. In: Advances in Agronomy. pp 111–178

Chen YT, Wang Y, Yeh KC (2017) Role of root exudates in metal acquisition and tolerance. Curr Opin Plant Biol 39:66–72. https://doi.org/10.1016/j.pbi.2017.06.004

Deer WA, Howie RA, Zussman J (2013) An Introduction to the Rock-Forming Minerals, 2nd edn. Mineralogical Society of Great Britain and Ireland

Degen T, Sadki M, Bron E, et al (2014) The HighScore suite. Powder Diffr 29:S13–S18. https://doi.org/10.1017/S0885715614000840

Döbelin N (2021) Profex: Open source XRD and Rietveld refinement. https://www.profex-xrd.org/. Accessed 26 Mar 2021

Doebelin N, Kleeberg R (2015) Profex: A graphical user interface for the Rietveld refinement program BGMN. J Appl Crystallogr 48:1573–1580. https://doi.org/10.1107/S1600576715014685

Du Laing G, De Vos R, Vandecasteele B, et al (2008) Effect of salinity on heavy metal mobility and availability in intertidal sediments of the Scheldt estuary. Estuar Coast Shelf Sci 77:589–602. https://doi.org/10.1016/j.ecss.2007.10.017

Du Laing G, Rinklebe J, Vandecasteele B, et al (2009) Trace metal behaviour in estuarine and riverine floodplain soils and sediments: A review. Sci Total Environ 407:3972–3985. https://doi.org/10.1016/j.scitotenv.2008.07.025

Eijkelkamp (2009) Redox measuring equipment: operating instructions

EU (2008a) Directive 2008/98/EC of the European Parliament and of the Council of 19 November 2008 on waste and repealing certain Directives. Official Journal of the European Communities. L312:59

EU (2008b) Directive 2008/58/EC of the European Parliament and of the Council of 17 June 2008 establishing a framework for community action in the field of marine environmental policy (Marine Strategy Framework Directive). Official Journal of the European Communitie. 27

Ferrans L, Schmieder F, Mugwira R, et al (2022) Dredged sediments as a plant-growing substrate: Estimation of health risk index. Sci Total Environ 846:157463. https://doi.org/10.1016/j.scitotenv.2022.157463

Ghobadi R, Altaee A, Zhou JL, et al (2021) Effective remediation of heavy metals in contaminated soil by electrokinetic technology incorporating reactive filter media. Sci Total Environ 794:148668. https://doi.org/10.1016/j.scitotenv.2021.148668

Gomes HI, Dias-Ferreira C, Ribeiro AB (2012) Electrokinetic remediation of organochlorines in soil: Enhancement techniques and integration with other remediation technologies. Chemosphere 87:1077–1090. https://doi.org/10.1016/j.chemosphere.2012.02.037

Han D, Wu X, Li R, et al (2021) Critical review of electro-kinetic remediation of contaminated soils and sediments: mechanisms, performances and technologies. Water Air Soil Pollut 232:335. https://doi.org/10.1007/s11270-021-05182-4

Heiri O, Lotter AF, Lemcke G (2001) Loss on ignition as a method for estimating organic and carbonate content in sediments: reproducibility and comparability of results. J Paleolimnol 25:101–110. https://doi.org/10.1023/A:1008119611481

Huang T, Li D, Kexiang L, Zhang Y (2015) Heavy metal removal from MSWI fly ash by electrokinetic remediation coupled with a permeable activated charcoal reactive barrier. Sci Rep 5:1–16. https://doi.org/10.1038/srep15412

Interreg ReCon Soil (2022) France (Channel Manche) England. Reconstructed Soils from Waste. ReCon Soil. https://www.channelmanche.com/en/projects/approved-projects/reconstructed-soils-from-waste/. Accessed 21 Nov 2022

ISO 10693 (1995) ISO 10693. https://www.iso.org/standard/18781.html

Kanbar HJ, Kaouk M (2019) Mineral and chemical changes of sediments after Cu sorption and then desorption induced by synthetic root exudate. Chemosphere 236:124393. https://doi.org/10.1016/j.chemosphere.2019.124393

Kanbar HJ, Matar Z, Safa GA-A, Kazpard V (2020) Selective metal leaching from technosols based on synthetic root exudate composition. J Environ Sci 96:85–92. https://doi.org/10.1016/j.jes.2020.04.040

Kanbar HJ, Srouji EE, Zeidan Z, et al (2018) Leaching of metals in coastal technosols triggered by saline solutions and labile organic matter removal. Water, Air, Soil Pollut 229:157. https://doi.org/10.1007/s11270-018-3808-z

Karaca O, Cameselle C, Reddy KR (2016) Electrokinetic Removal of Heavy Metals from Mine Tailings and Acid Lake Sediments from Can Basin, Turkey. In: Geo-Chicago 2016. pp 225–234

Kaviany M (1995) Principles of Heat Transfer in Porous Media, 2nd edn. Springer New York, New York, NY

Ketelaars M, Hommes S, Reinders J, et al (2013) The beneficial re-use of dredged material

Kiani M, Raave H, Simojoki A, et al (2021) Recycling lake sediment to agriculture: Effects on plant growth, nutrient availability, and leaching. Sci Total Environ 753:141984. https://doi.org/10.1016/j.scitotenv.2020.141984

Kim DH, Jo SU, Yoo JC, Baek K (2013) Ex situ pilot scale electrokinetic restoration of saline soil using pulsed current. Sep Purif Technol 120:282–288. https://doi.org/10.1016/j.seppur.2013.10.007

Klitzke S, Lang F (2009) Mobilization of soluble and dispersible lead, arsenic, and antimony in a polluted, organic-rich soil - Effects of pH increase and counterion valency. J Environ Qual 38:933–939. https://doi.org/10.2134/jeq2008.0239

Kristensen E, Ahmed SI, Devol AH (1995) Aerobic and anaerobic decomposition of organic matter in marine sediment: Which is fastest? Limnol Oceanogr 40:1430–1437. https://doi.org/10.4319/lo.1995.40.8.1430

Lee S, Roh Y, Koh DC (2019) Oxidation and reduction of redox-sensitive elements in the presence of humic substances in subsurface environments: A review. Chemosphere 220:86–97. https://doi.org/10.1016/j.chemosphere.2018.11.143

Li D, Tan XY, Wu X Da, et al (2014) Effects of electrolyte characteristics on soil conductivity and current in electrokinetic remediation of lead-contaminated soil. Sep Purif Technol 135:14–21. https://doi.org/10.1016/j.seppur.2014.07.048

Li F, Liang N, Zhang P, et al (2018) Protection of extractable lipid and lignin: Differences in undisturbed and cultivated soils detected by molecular markers. Chemosphere 213:314–322. https://doi.org/10.1016/j.chemosphere.2018.09.043

Li H, Shi A, Li M, Zhang X (2013) Effect of pH, temperature, dissolved oxygen, and flow rate of overlying water on heavy metals release from storm sewer sediments. J Chem 2013:1–11. https://doi.org/10.1155/2013/434012

Li T, Yuan S, Wan J, et al (2009) Pilot-scale electrokinetic movement of HCB and Zn in real contaminated sediments enhanced with hydroxypropyl-β-cyclodextrin. Chemosphere 76:1226–1232. https://doi.org/10.1016/j.chemosphere.2009.05.045

LIFE SEDI.PORT.SIL (2021) Recovery of dredged SEDIments of the PORT of Ravenna and SILicon extraction. In: Eur. Comm. LIFE Public Database

Liu X, Xu L, Zhuang Y (2023) Effect of electrolyte, potential gradient and treatment time on remediation of hexavalent chromium contaminated soil by electrokinetic remediation and adsorption. Environ Earth Sci 82:40. https://doi.org/10.1007/s12665-022-10673-6

López-Vizcaíno R, dos Santos E V., Yustres A, et al (2019) Calcite buffer effects in electrokinetic remediation of clopyralid-polluted soils. Sep Purif Technol 212:376–387. https://doi.org/10.1016/j.seppur.2018.11.034

López-Vizcaíno R, Yustres A, León MJ, et al (2017) Multiphysics implementation of electrokinetic remediation models for natural soils and porewaters. Electrochim Acta 225:93–104. https://doi.org/10.1016/j.electacta.2016.12.102

Lu P, Feng Q, Meng Q, Yuan T (2012) Electrokinetic remediation of chromium- and cadmium-contaminated soil from abandoned industrial site. Sep Purif Technol 98:216–220. https://doi.org/10.1016/j.seppur.2012.07.010

Lynch S, Batty L, Byrne P (2014) Environmental risk of metal mining contaminated river bank sediment at redox-transitional zones. Minerals 4:52–73. https://doi.org/10.3390/min4010052

Marshak S (2011) Streams and floods: The geology of running water. In: Repcheck J (ed) Earth: Portrait of a Planet, 2nd edn. W.W. Norton & Company, New York and London, pp 582–619

McBride MB, Pitiranggon M, Kim B (2009) A comparison of tests for extractable copper and zinc in metal-spiked and field-contaminated soil. Soil Sci 174:439–444. https://doi.org/10.1097/SS.0b013e3181b66856

Mertens J, Smolders E (2013) Zinc. In: Alloway BJ (ed) Heavy Metals in Soils: Trace Metals and Metalloids in Soils and their Bioavailability, 3rd edn. Springer Dordrecht, pp 465–493

Micic S, Shang JQ, Lo KY, et al (2001) Electrokinetic strengthening of a marine sediment using intermittent current. Can Geotech J 38:287–302. https://doi.org/10.1139/cgj-38-2-287

Miranda LS, Ayoko GA, Egodawatta P, et al (2021) Physico-chemical properties of sediments governing the bioavailability of heavy metals in urban waterways. Sci Total Environ 763:142984. https://doi.org/10.1016/j.scitotenv.2020.142984

Neaman A, Selles I, Martínez CE, Dovletyarova EA (2020) Analyzing soil metal toxicity: spiked or field-contaminated soils? Environ Toxicol Chem 39:513–514. https://doi.org/10.1002/etc.4654

Ortiz-Soto R, Leal D, Gutierrez C, et al (2023) Incidence of electric field and sulfuric acid concentration in electrokinetic remediation of Cobalt, Copper, and Nickel in fresh copper mine tailings. Processes 11:108. https://doi.org/10.3390/pr11010108

Ouhadi VR, Yong RN, Shariatmadari N, et al (2010) Impact of carbonate on the efficiency of heavy metal removal from kaolinite soil by the electrokinetic soil remediation method. J Hazard Mater 173:87–94. https://doi.org/10.1016/j.jhazmat.2009.08.052

Owens PN, Batalla RJ, Collins AJ, et al (2005) Fine-grained sediment in river systems: Environmental significance and management issues. River Res Appl 21:693–717. https://doi.org/10.1002/rra.878

Pedersen KB, Benamar A, Ammami M, et al (2021) Electrokinetic Remediation of Dredged Contaminated Sediments. Electrokinet Remediat Environ Secur Sustain 99–139.

https://doi.org/10.1002/9781119670186.ch5

Poppe LJ, Paskevich VF, Hathaway JC, Blackwood DS (2001) A Laboratory Manual for X-Ray Powder Diffraction

Post JE, Bish DL (1989) Rietveld refinement of crystal structures using powder X-ray diffraction data. Mod Powder Diffr 20:277–308

Reddy KR, Chinthamreddy S (1999) Electrokinetic remediation of heavy metal-contaminated soils under reducing environments. Waste Manag 19:269–282. https://doi.org/10.1016/S0956-053X(99)00085-9

Roberts D, Nachtegaal M, Sparks DL (2005) Speciation of Metals in Soils. In: Tabatabai MA, Sparks DL (eds) Chemical Processes in Soils. Soil Science Society of America, Madison, WI, pp 619–654

Song Y, Ammami M, Benamar A, et al (2016) Effect of EDTA, EDDS, NTA and citric acid on electrokinetic remediation of As, Cd, Cr, Cu, Ni, Pb and Zn contaminated dredged marine sediment. Environ Sci Pollut Res 23:10577–10586. https://doi.org/10.1007/s11356-015-5966-5

Sun Z, Zhao M, Chen L, et al (2023) Electrokinetic remediation for the removal of heavy metals in soil: Limitations, solutions and prospection. Sci Total Environ 903:165970. https://doi.org/10.1016/j.scitotenv.2023.165970

Tian F, Hou M, Qiu Y, et al (2020) Salinity stress effects on transpiration and plant growth under different salinity soil levels based on thermal infrared remote (TIR) technique. Geoderma 357:113961. https://doi.org/10.1016/j.geoderma.2019.113961

Torrance K, João E, Lord R (2008) Dredged Sediment; Waste or Resource?

Van Driessche AES, Stawski TM, Kellermeier M (2019) Calcium sulfate precipitation pathways in natural and engineered environments. Chem Geol 530:119274. https://doi.org/10.1016/j.chemgeo.2019.119274

Vanysek P (1993) Ionic conductivity and diffusion at infinite dilution. CRC hand B Chem Phys 5–92

Wang Y, Han Z, Li A, Cui C (2021) Enhanced electrokinetic remediation of heavy metals contaminated soil by biodegradable complexing agents. Environ Pollut 283:117111. https://doi.org/10.1016/j.envpol.2021.117111

Wen D, Fu R, Li Q (2021a) Removal of inorganic contaminants in soil by electrokinetic remediation technologies: A review. J Hazard Mater 401:123345. https://doi.org/10.1016/j.jhazmat.2020.123345

Wen D, Guo X, Fu R (2021b) Inhibition characteristics of the electrokinetic removal of inorganic contaminants from soil due to evolution of the acidic and alkaline fronts. Process Saf Environ Prot 155:343–354. https://doi.org/10.1016/j.psep.2021.09.030

Wierzba S, Makuchowska-Fryc J, Kłos A, et al (2022) Role of calcium carbonate in the process of heavy metal biosorption from solutions: synergy of metal removal mechanisms. Sci Rep 12:1–13. https://doi.org/10.1038/s41598-022-22603-4

Wu J, Zhang J, Xiao C (2016) Focus on factors affecting pH, flow of Cr and transformation between Cr(VI) and Cr(III) in the soil with different electrolytes. Electrochim Acta 211:652–662. https://doi.org/10.1016/j.electacta.2016.06.048

Xu H, Bai J, Yang X, et al (2022) Lab scale-study on the efficiency and distribution of energy consumption in chromium contaminated aquifer electrokinetic remediation. Environ Technol Innov 25:102194. https://doi.org/10.1016/j.eti.2021.102194

Xu Y, Liao Y, Lin Z, et al (2019) Precipitation of calcium sulfate dihydrate in the presence of fulvic acid and magnesium ion. Chem Eng J 361:1078–1088. https://doi.org/10.1016/j.cej.2019.01.003

Yan Y, Wan B, Mansor M, et al (2022) Co-sorption of metal ions and inorganic anions/organic ligands on environmental minerals: A review. Sci Total Environ 803:149918. https://doi.org/10.1016/j.scitotenv.2021.149918

Yeung AT, Gu YY (2011) A review on techniques to enhance electrochemical remediation of contaminated soils. J Hazard Mater 195:11–29. https://doi.org/10.1016/j.jhazmat.2011.08.047

Zein-Eddin A, Kanbar HJ, Ammami MT, Benamar A (2023) Physico-chemical, mineral, and chemical variation of dredged sediments caused by electrokinetic remediation. Preprint at ResearchSquare. https://doi.org/https://doi.org/10.21203/rs.3.rs-2763002/v1

Zhang Y, Labianca C, Chen L, et al (2021) Sustainable ex-situ remediation of contaminated sediment: A review. Environ Pollut 287:117333. https://doi.org/10.1016/j.envpol.2021.117333

Zhou DM, Cang L, Alshawabkeh AN, et al (2006) Pilot-scale electrokinetic treatment of a Cu contaminated red soil. Chemosphere 63:964–971. https://doi.org/10.1016/j.chemosphere.2005.08.059

DOI: 10.1007/s11356-023-30271-8
Published in Environmental Science and Pollution Research

Supplementary Materials

Electrokinetic remediation of estuarine sediments using a large reactor: Spatial variation of physicochemical, mineral, and chemical properties

Hussein J. Kanbar*, Ahmad Zein-Eddin, Mohamed-Tahar Ammami, Ahmed Benamar

Laboratoire Ondes et Milieux complexes (LOMC), UMR 6294 CNRS, University of Le Havre Normandy (ULHN), 76600 Le Havre, France

* Correspondence: Hussein J. Kanbar, Hsen.kanbar@gmail.com, ORCID: 0000-0002-9505-9974; Mohamed-Tahar Ammami, mohamed-tahar.ammami@univ-lehavre.fr

Content

DOI: 10.1007/s11356-023-30271-8
Published in Environmental Science and Pollution Research

SM 1: ANOVA and post-hoc Tukey's HSD (honestly significant difference) test

The physicochemical parameters of the sediment porewater (PW) did not show any significant variation with compartments (L and R), depths (z1: 0 – 13.3 cm, z2: 13.3 – 26.6 cm, and z3: 26.6 – 40 cm), or widths (y1: 0 – 13.3 cm, y2: 13.3 – 26.6 cm, and y3: 26.6 – 40 cm) (ANOVA, table below). This indicates that the variation is only based on the anode-cathode direction (lengthwise); width, depth, and compartment had no significant effect on those parameters.

ANOVA results

Source	Dependent Variable	*P*
Width (y1, y2, and y3)	pH	.966
	EC	.938
Depth (z1, z2, and z3)	pH	.679
	EC	.640
Compartment (L and R)	pH	.447
	EC	.688
Width * Depth	pH	.974
	EC	.990
Width * Compartment	pH	.787
	EC	.970
Depth * Compartment	pH	.795
	EC	.998
Width * Depth * Compartment	pH	.969
	EC	.989

P: *P* value. The *P* value is the probability of finding the observed results when the null hypothesis (H_0) is true. H_0: there is no significant difference of the dependent variables as a function of parameter (width, depth, and compartment)

Furthermore, the similarity of porewater pH and EC is identified by Tukey's HSD test as a function of width and depth.

Test of significance: porewater pH as a function of width

	Width	N	Subset 1
Tukey HSD[a,b]	y1	36	8.6414
	y2	36	8.7219
	y3	36	8.8242
	Sig.		.965

Means for groups in homogeneous subsets are displayed.
Based on observed means.
The error term is Mean Square (Error) = 9.367.
a. Uses Harmonic Mean Sample Size = 36.000.
b. Alpha = .05

Test of significance: porewater EC as a function of width

	Width	N	Subset 1
Tukey HSD[a,b]	y1	36	17.0856
	y2	36	17.5008
	y3	36	18.0175
	Sig.		.933

Means for groups in homogeneous subsets are displayed.
Based on observed means.
The error term is Mean Square (Error) = 123.821.
a. Uses Harmonic Mean Sample Size = 36.000.
b. Alpha = .05

DOI: 10.1007/s11356-023-30271-8
Published in Environmental Science and Pollution Research

Test of significance: porewater pH as a function of depths

	Depth	N	Subset 1
Tukey HSD[a,b,c]	z1	30	8.3600
	z2	42	8.7376
	z3	36	9.0269
	Sig.		.632

Means for groups in homogeneous subsets are displayed.
Based on observed means.
The error term is Mean Square (Error) = 9.367.
a. Uses Harmonic Mean Sample Size = 35.327.
b. The group sizes are unequal. The harmonic mean of the group sizes is used. Type I error levels are not guaranteed.
c. Alpha = .05.

Test of significance: porewater EC as a function of depths

	Depth	N	Subset 1
Tukey HSD[a,b,]	z1	36	16.1725
	z2	30	17.7553
	z3	42	18.5445
	Sig.		.644

Means for groups in homogeneous subsets are displayed.
Based on observed means.
The error term is Mean Square (Error) = 123.821.
a. Uses Harmonic Mean Sample Size = 35.327.
b. The group sizes are unequal. The harmonic mean of the group sizes is used. Type I error levels are not guaranteed.
c. Alpha = .05.

DOI: 10.1007/s11356-023-30271-8
Published in Environmental Science and Pollution Research

SM 2: Oriented XRD

From the oriented and air-dried slide (figure below), it is clear that the sediment contains illite (10 Å). The persistence of this peak at 10 Å for the ethylene glycolated (EG) and calcinated (550°C) samples indicates illite. Other minerals that were identified by the oriented slides are possibly vermiculite, smectites, kaolinite, and/or other clay minerals with 14 and 7 Å d-spacings. The 7.14 Å peak might belong to kaolinite (d010), montmorillonite (d002), chlorite (d002), or vermiculite (d004). The presence of kaolinite is confirmed by the presence of the diffraction peaks at 7.14 and 3.58 Å (001 and 002 reflections, respectively), by the collapse of the 7.14 Å peak upon heating at 550°C, and by the anti-symmetrical stretching bands of external and internal OH at 3697 and 3620 cm^{-1} revealed by infrared (Madejová et al. 2017) (*SM 3*).

The 14 Å peak collapsed a little after heating at 400°C, indicating vermiculite or montmorillonite. Montmorillonite is possibly present since this peak formed a broad peak after EG (due to swelling). The 060 peaks at ~1.54 and 1.50 Å (*Fig 6*a in the main text) indicate trioctahedral and dioctahedral phyllosilicates (e.g., chlorite, vermiculite, interlayered illite-vermiculite, illite-montmorillonite), respectively (Brown and Brindley 1980; MacEwan and Wilson 1980; Poppe et al. 2001). Vermiculite 002 (14 Å) spacing increases after EG, but not as much as montmorillonite. However, the 001 (or 002) peak remained after heating, indicating chlorite (this peak collapses to 10 Å for vermiculite and smectites). Therefore, this peak (001 or 002) indicates chlorite, vermiculite, or montmorillonite (or all three). Furthermore, the 7 Å (002) of chlorite collapses after calcination. The collapse of the 14 Å peak to 10 Å further indicates trioctahedral vermiculite or trioctahedral montmorillonite. The sharpening of the 10 Å peak after 400°C treatment indicates interstratified illite-montmorillonite or illite-vermiculite. The 001 spacing at 14 Å swelled to 14-18 Å, indicating a mixture of swelling and non-swelling clay minerals, such as illite/montmorillonite (i.e., illite/smectite), vermiculite/chlorite, illite/vermiculite, and/or chlorite/montmorillonite. Indeed, the 14 Å peak of interstratified illite-vermiculite minerals remains after EG and collapses to 10 Å after calcination; while that of illite-montmorillonite expands after EG and collapses to 10 Å after calcination; thus, explaining the presence of peaks at 14.3 Å as well as 17 Å after EG (some swelling and others non-swelling minerals).

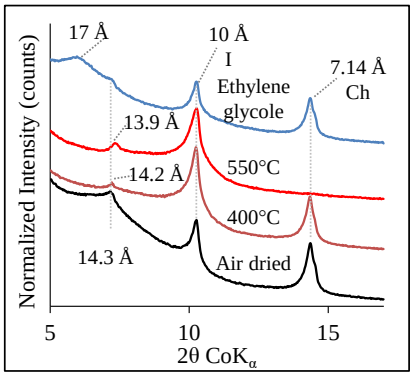

DOI: 10.1007/s11356-023-30271-8
Published in Environmental Science and Pollution Research

SM 3: Infrared spectroscopy

The dissolution of carbonates in the sediments near the anode was detected by infrared (IR) spectra through the decrease in the peak intensities at 874, 1435, 1800, and 2520 cm^{-1} and the shoulder at 2600 cm^{-1} (Vogel et al. 2008; De Lorenzi Pezzolo 2013; So et al. 2020) (figure below).

The presence of the Si-O stretching band at ~1032 cm^{-1} indicates silicates (phyllosilicates), such as illite/montmorillonite, vermiculite (*Fig 6* and *SM 2*). The change in the stretching Si-O vibration peaks significantly depends on the chemical composition and structural characteristics of clay minerals (Madejová et al. 2017). This peak shifted to smaller wavenumbers especially for sediments 30 cm away from the anode (figure below). The shift in the Si-O peak away from 1032 cm^{-1} indicates that Si-O gets occupied with possible cations in the porewater (Yesilbas et al. 2018; Lindholm et al. 2019).

Furthermore, the edge of the ~1042 cm^{-1} peak for the sediments near the anode (~0 – 10 cm) was to the left (higher wavenumbers) of the initial sediment, while it shifted to lower wavenumbers for samples towards the cathode. The same applies to the peak at 1012 cm^{-1}.

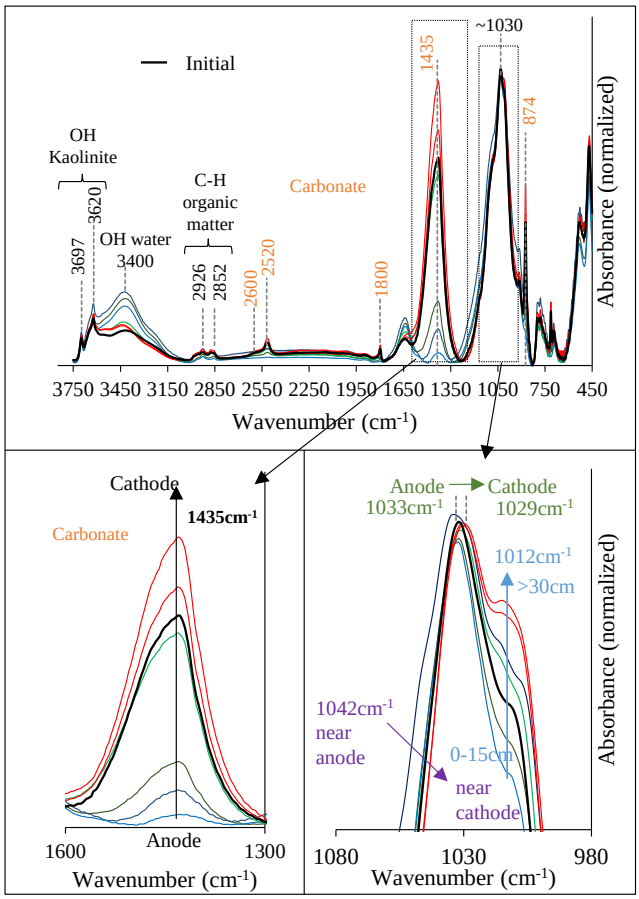

DOI: 10.1007/s11356-023-30271-8
Published in Environmental Science and Pollution Research

SM 4: Visual MINTEQ elemental species

The possible metal species in the sediment's porewater (after treatment) as a function of pH. The data was generated using Visual MINTEQ, version 3.1.

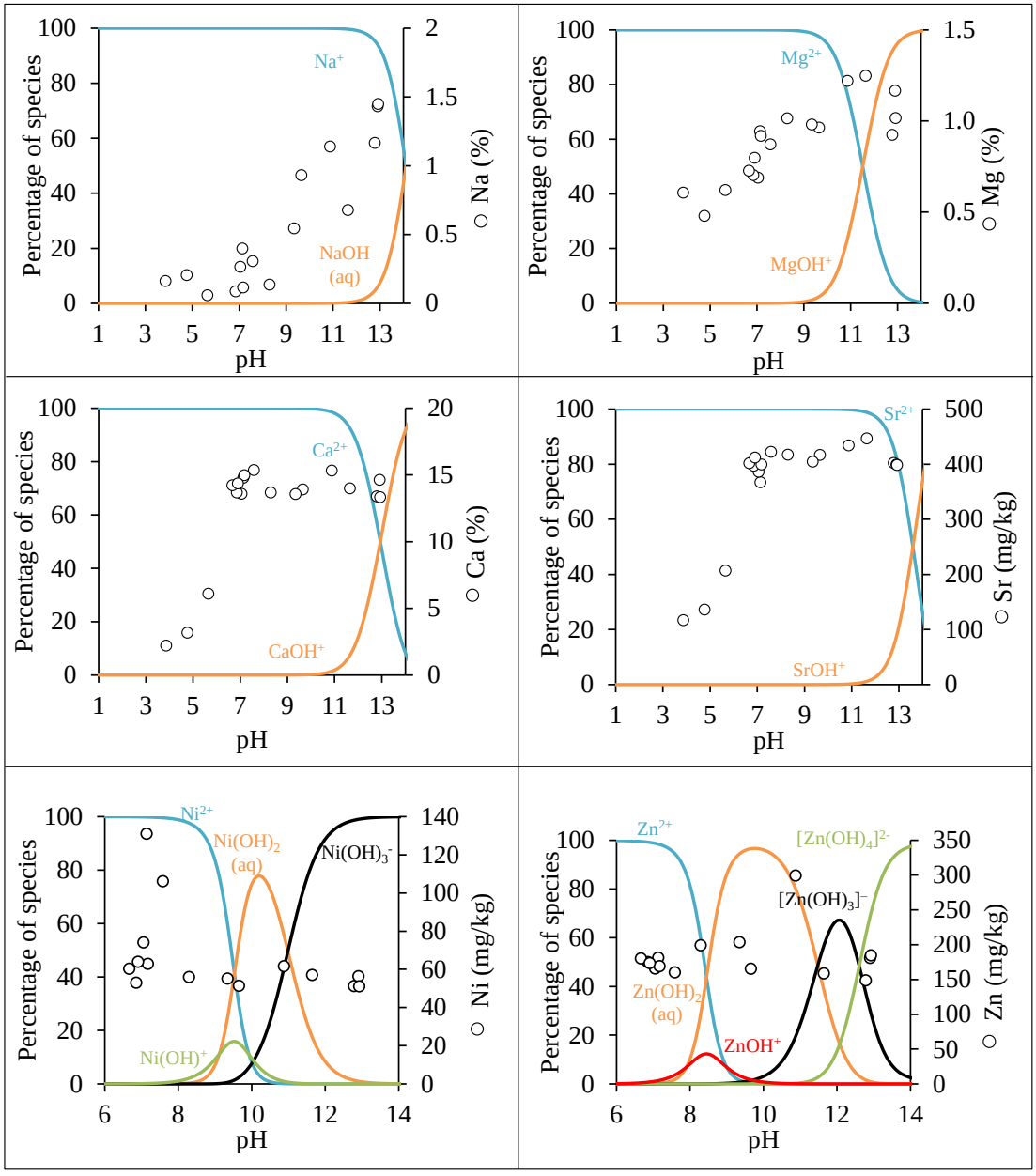

DOI: 10.1007/s11356-023-30271-8
Published in Environmental Science and Pollution Research

References

Brown G, Brindley GW (1980) X-ray diffraction procedures for clay mineral identification. In: Brindley GW, Brown G (eds) Crystal structures of clay minerals and their X-ray identification. Mineralogical Society, London, pp 305–359

De Lorenzi Pezzolo A (2013) An exercise on calibration: DRIFTS study of binary mixtures of calcite and dolomite with partially overlapping spectral features. J Chem Educ 90:118–122. https://doi.org/10.1021/ed2008729

Lindholm J, Boily JF, Holmboe M (2019) Deconvolution of smectite hydration isotherms. ACS Earth Sp Chem 3:2490–2498. https://doi.org/10.1021/acsearthspacechem.9b00178

MacEwan DMC, Wilson MJ (1980) Interlayer and intercalation complexes of clay minerals. In: Brindley GW, Brown G (eds) Crystal structures of clay minerals and their X-ray identification. Monograph, pp 197–248

Madejová J, Gates WP, Petit S (2017) IR spectra of clay minerals. In: Gates WP, Kloprogge JT, Madejová J, Bergaya F (eds) Developments in Clay Science. Eslevier, pp 107–149

Poppe LJ, Paskevich VF, Hathaway JC, Blackwood DS (2001) A Laboratory Manual for X-Ray Powder Diffraction

So RT, Blair NE, Masterson AL (2020) Carbonate mineral identification and quantification in sediment matrices using diffuse reflectance infrared Fourier transform spectroscopy. Environ Chem Lett 18:1725–1730. https://doi.org/10.1007/s10311-020-01027-4

Vogel H, Rosén P, Wagner B, et al (2008) Fourier transform infrared spectroscopy, a new cost-effective tool for quantitative analysis of biogeochemical properties in long sediment records. J Paleolimnol 40:689–702. https://doi.org/10.1007/s10933-008-9193-7

Yesilbas M, Holmboe M, Boily JF (2018) Cohesive vibrational and structural depiction of intercalated water in montmorillonite. ACS Earth Sp Chem 2:38–47. https://doi.org/10.1021/acsearthspacechem.7b00103